Interaction Notes

Note 323

Transmission Through One or More Small Apertures of Arbitrary Shape

September 1977

D.L. Jaggard
California Institute of Technology

Abstract

The transmission through one or more electrically small apertures of arbitrary shape located in a planar electrical wall is investigated. The orientation of the incident fields for minimum and maximum transmission is discussed. Through the use of equivalent inner and outer radii, lower and upper bounds are found for the electric and mean magnetic aperture polarizabilities. As a result upper and lower bounds and approximations are found for the transmission coefficient of single apertures of arbitrary shape. Plots are also given of the energy distribution in typical cases. A rule is given for the ordering of aperture transmission according to shape for small convex apertures. These results are extended to include transmission through many apertures in a linear array. It is found that coupling among apertures can either increase or decrease the transmission per aperture depending upon the relative orientation of the incident magnetic field with the line of the aperture array. A numerical example demonstrates these concepts for the case of grazing incidence.

ACKNOWLEDGMENT

The author thanks Professor C. H. Papas of the California Institute of Technology for many informative discussions and helpful insights during the course of this research. Dr. K.S.H. Lee of Dikewood Industries initially suggested this problem and provided encouragement and suggestions throughout the project.

SECTION I
INTRODUCTION

The problem of electromagnetic coupling through a small circular aperture was apparently first solved by Bethe [1] in an approximate manner. The scattered field was found to be equivalent to the field of electric and magnetic dipole sources located at the center of the aperture where the electric dipole was proportional to the normal electric field and the magnetic dipole was proportional to the tangential magnetic field. The derivation was based on electrostatic and magnetostatic approximations of the fields in the aperture. Figure 1 shows how the transmitted fields are similar to those produced by electric and magnetic dipole moments $\underline{p}_e$ and $\underline{p}_m$.

An exact solution [2,3,4] was found to agree with the Bethe result in the far field. However, the near field of the approximate Bethe solution does not satisfy the edge condition [2,3,5,6] and has an incorrect coordinate dependance near the aperture.

In this report the amount and distribution of energy transmitted through one or more small apertures are of interest. In section II the approximate and exact solution in the near field are compared. Plots are given of the energy distribution. The problem of noncircular apertures is discussed in section III which includes the special cases of elliptical, rectangular, triangular and rhombical shapes. The analysis uses the notions of inner and outer radii which were recently used by Papas in similar calculations [7]. Section IV contains a useful approximation for the coupling between two small apertures of arbitrary shape. The effect of many small apertures is examined briefly in section V. An application for the case of grazing incidence is given in section VI. Section VII contains comments and conclusions.

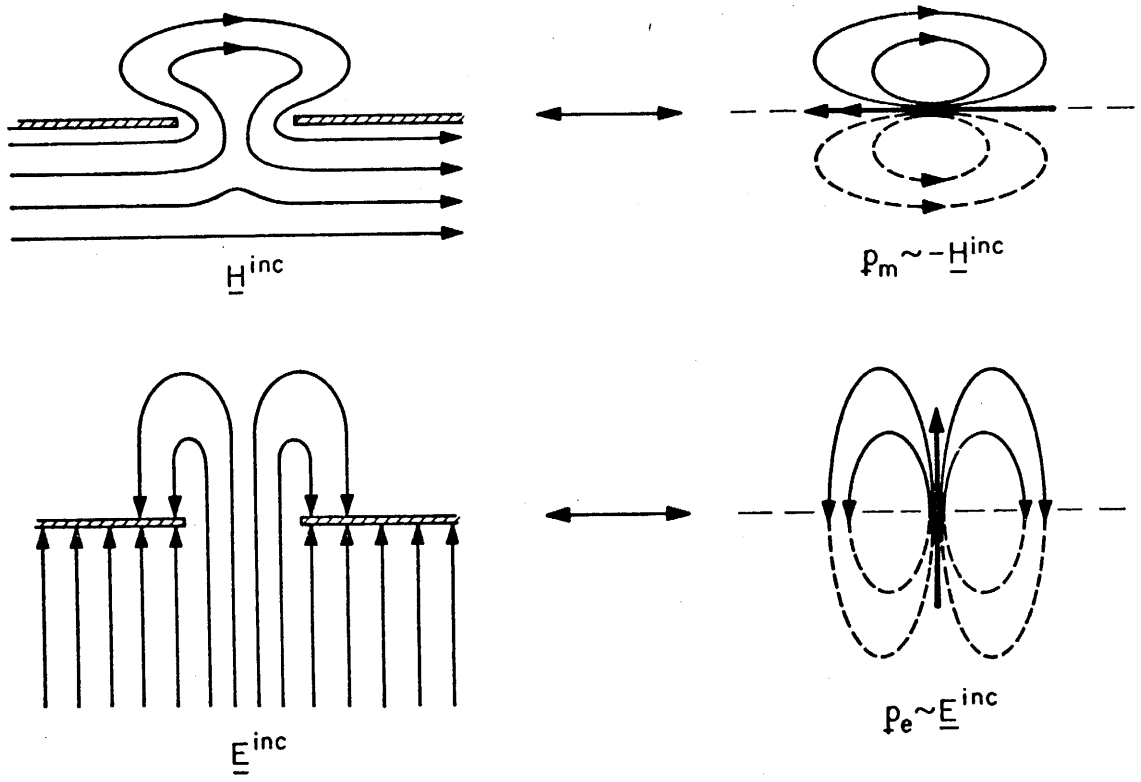

Figure 1. Sketch Showing the Equivalence of Small Hole Radiation and Radiation From Electric and Magnetic Dipole Moments $\underline{p}_e$ and $\underline{p}_m$. The dipole radiation shown is valid for fields on the shadow side of the small hole (solid lines). Oppositely directed dipoles produce the correct scattered field on the illuminated side of the small hole.

SECTION II
TRANSMISSION THROUGH SMALL CIRCULAR APERTURES

The Bethe result is most easily obtained through consideration of the complementary disk problem and a subsequent application of Babinet's principle. The electric and magnetic susceptibilities χ^e and χ^m can be found for metallic circular disks of radius a [8]. For the electric and magnetic fields normal to a disk of radius a we have, respectively,

$$\left.\begin{aligned} \chi^e_{disk} &= 0 \\ \chi^m_{disk} &= -\frac{8}{3}\mu_o a^3 \end{aligned}\right\} \qquad (1)$$

where μ_o = permeability of free space

For tangential electric and magnetic fields we have

$$\left.\begin{aligned} \chi^e_{disk} &= \frac{16}{3}\varepsilon_o a^3 \\ \chi^m_{disk} &= 0 \end{aligned}\right\} \qquad (2)$$

where ε_o = permittivity of free space

The susceptibilities are defined by the ratios of the electric and magnetic dipole moments to their respective incident (traveling-wave) field amplitudes E^{inc} and H^{inc}. The incident fields vary as $e^{i(\underline{k}\cdot\underline{r}-\omega t)}$.

$$\chi^e = p_e / E^{inc}$$

$$\chi^m = p_m / H^{inc} \tag{3}$$

For the case of circular apertures, we can find the dipole moments through Babinet's principle and the use of electromagnetic duals,

$$\underline{p}_e = \sin\alpha \frac{8}{3} \varepsilon_o a^3 \underline{E}^{inc} \hat{e}_n \tag{4}$$

$$\underline{p}_m = -\cos\beta \frac{16}{3} \mu_o a^3 \underline{H}^{inc} \hat{e}_\perp \tag{5}$$

where

$$\sin\alpha = (\underline{E}^{inc} \times \hat{e}_{||}) \cdot \hat{e}_\perp / E^{inc}$$

$$\cos\beta = \underline{H}^{inc} \cdot \hat{e}_\perp / H^{inc}$$

For parallel polarization $\beta = 0$ and for perpendicular polarization $\alpha = 0$. The right-handed coordinate system formed by the triad of unit vectors $\hat{e}_{||}$, $\hat{e}_\perp$ and $\hat{e}_n$ is shown in figure 2. The transmitted fields E^{tr} and H^{tr} are found as a function of the dipole moments (and hence the incident fields) and the spherical coordinates (r,θ,ϕ) from Papas [9].

$$E_r^{tr} = \frac{1}{\varepsilon_o} p_e \cos\theta \left(-\frac{2ik}{r} + \frac{2}{r^2} \right) G \tag{6}$$

$$E_\theta^{tr} = -\frac{1}{\varepsilon_o} p_e \sin\theta \left(\frac{ik}{r} - \frac{1}{r^2} + k^2 \right) G - i\omega p_m \cos\phi \left(ik - \frac{1}{r} \right) G \tag{7}$$

$$E_\phi^{tr} = i\omega p_m \cos\theta \sin\phi \left(ik - \frac{1}{r} \right) G \tag{8}$$

$$H_r^{tr} = \frac{1}{\mu_o} p_m \sin\theta \sin\phi \left(\frac{-2ik}{r} + \frac{2}{r^2} \right) G \tag{9}$$

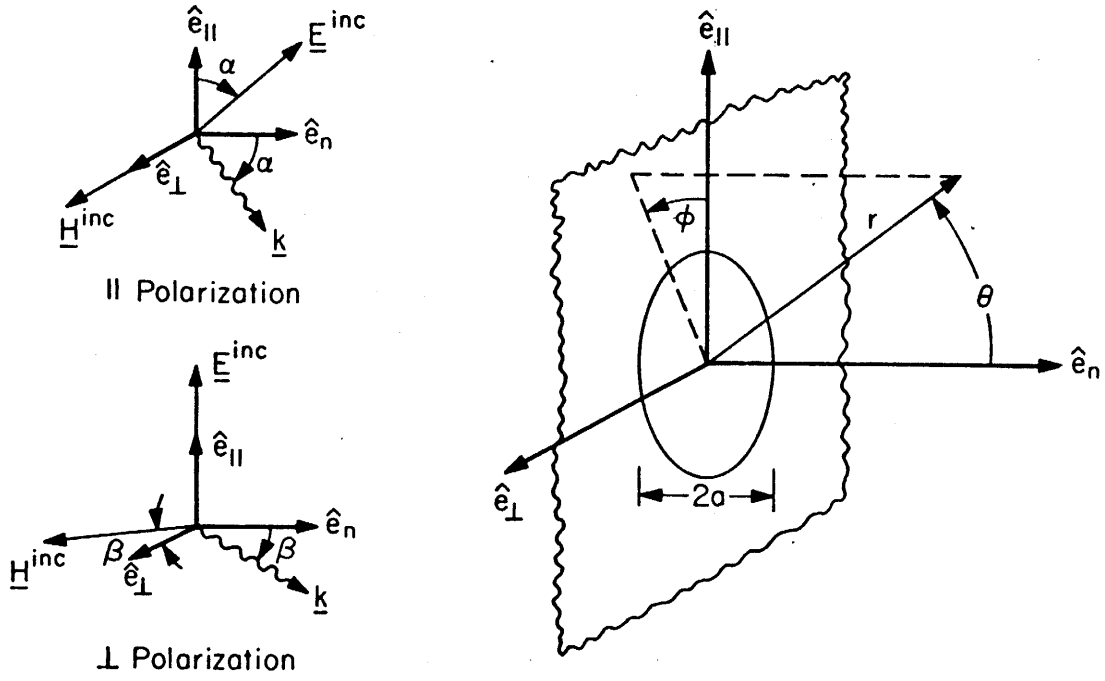

Figure 2. Geometry of Incident Fields and Circular Aperture for Parallel and Perpendicular Polarization.

$$H_\theta^{tr} = \frac{1}{\mu_o} p_m \cos\theta \sin\phi \left(\frac{ik}{r} - \frac{1}{r^2} + k^2\right) G \tag{10}$$

$$H_\phi^{tr} = i\omega p_e \sin\theta \left(ik - \frac{1}{r}\right) G + \frac{1}{\mu_o} p_m \cos\phi \left(\frac{ik}{r} - \frac{1}{r^2} + k^2\right) G \tag{11}$$

where

$G = e^{ikr}/4\pi r$ $\quad$ r = radial distance from origin

$k = \omega/c = 2\pi/\lambda$ $\quad$ θ = polar angle from $\hat{e}_n$

c = vacuum speed of light $\quad$ ϕ = azimuthal angle from $\hat{e}_{||}$

λ = vacuum wavelength

ω = radian frequency

and where the time dependence $e^{-i\omega t}$ has been suppressed. This result is identical to Bethe's approximation [1].

We now consider the total energy density in the near field (i.e., $r \ll \lambda$) as computed from the above equations. The time-averaged energy density $\overline{w}$ is defined by

$$\overline{w} = \overline{w}_e + \overline{w}_m \tag{12}$$

where

$$\overline{w}_e = \frac{\varepsilon_o}{4} \underline{E} \cdot E^* \tag{13}$$

$$\overline{w}_m = \frac{\mu_o}{4} \underline{H} \cdot \underline{H}^* \tag{14}$$

The ratio of the near-field transmitted energy density to the incident energy density can be computed as

$$\frac{\overline{w}^{tr}}{\overline{w}^{inc}} = \frac{2}{9\pi^2} \left(\frac{a}{r}\right)^6 \begin{cases} 4\cos^2\beta(4\sin^2\theta\sin^2\phi + \cos^2\theta\sin^2\phi + \cos^2\phi) & \perp \text{ polarization} \\ 4(4\sin^2\theta\sin^2\phi + \cos^2\theta\sin^2\phi + \cos^2\phi) + \sin^2\alpha(4\cos^2\theta + \sin^2\theta) & || \text{ polarization} \end{cases}$$

for $r \ll \lambda$ (15)

where

$$\bar{w}^{inc} = \frac{\varepsilon_o}{4} \underline{E}^{inc} \cdot \underline{E}^{inc*} + \frac{\mu_o}{4} \underline{H}^{inc} \cdot \underline{H}^{inc*} = \frac{\varepsilon_o}{2} |E^{inc}|^2$$

The first term of (15) is due to the electric energy; whereas the second term is due to the magnetic energy. Therefore it is apparent that most of the near-field energy is magnetic in nature. This is due to the fact that for all polarizations the magnetic dipole contribution dominates the contribution from the electric dipole. Plots of the relative transmitted energy density in the E-plane ($\phi = 0, \pi$) and the H-plane ($\phi = \pm\pi/2$) are given as a function of θ for a constant value of r/a in figure 3. Several items concerning the transmitted energy in the near field should be noted from this figure:

1. maximum energy transmission for all polarizations occurs at the the intersection of the H-plane and the aperture plane ($\phi = \pm\pi/2$, $\theta = \pi/2$)
2. maximum energy transmission occurs for the case of parallel polarization and grazing incidence ($\alpha = \pi/2$, $\beta = 0$)
3. minimum (zero) energy transmission occurs for perpendicular polarization at grazing incidence ($\alpha = 0$, $\beta = \pi/2$)
4. for any given angles θ and ϕ, parallel polarization always produces an equal or larger energy transmission than does perpendicular polarization
5. the distribution of energy as a function of θ is relatively independent of the polarization of the incident wave.

The previous results will be compared with the exact calculations of Bouwkamp [2,3] for the case of normal incidence. For this comparison we note the ratio of the transmitted energy density to the incident energy

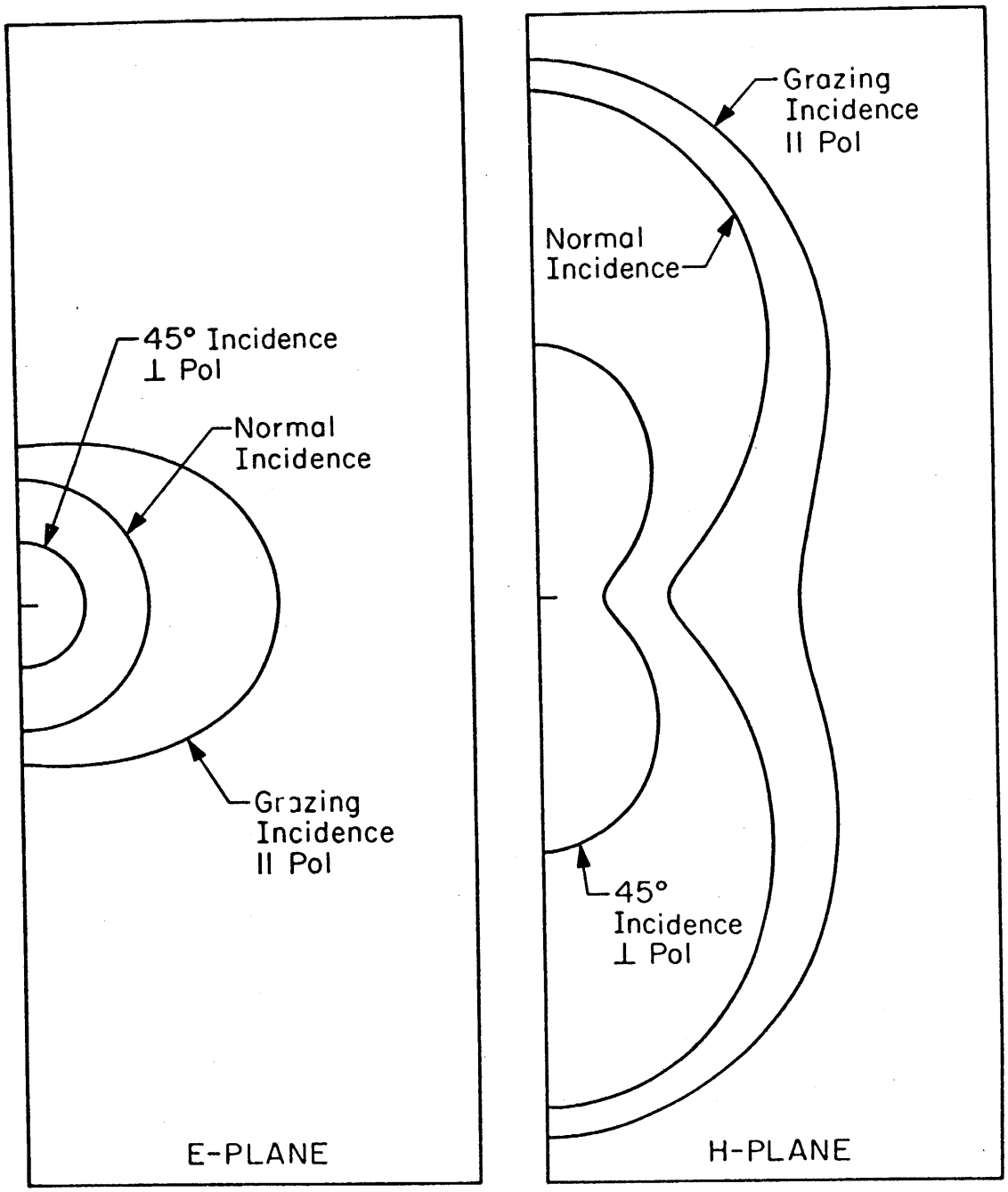

Figure 3. Relative Energy Distribution in the Near Field of a Small Circular Aperture. Note the symmetry with respect to the aperture normal. Maximum energy density in the H-plane occurs at the aperture plane.

density along the three coordinate axes. Bouwkamp's exact expression for this ratio is

$$\left(\frac{\bar{w}^{tr}}{\bar{w}^{inc}}\right)_{exact} = \frac{2}{\pi^2}\begin{cases}\left[\operatorname{arccot}\sqrt{\tilde{r}^2-1} - \dfrac{1}{\sqrt{\tilde{r}^2-1}}\left(1 - \dfrac{1}{\tilde{r}^2}\right)\right]^2 & r \text{ along } \hat{e}_{\|} \\ \left[\operatorname{arccot}\sqrt{\tilde{r}^2-1} - \dfrac{1}{\sqrt{\tilde{r}^2-1}}\left(1 + \dfrac{1}{\tilde{r}^2}\right)\right]^2 & r \text{ along } \hat{e}_{\perp} \\ \left[\operatorname{arccot}\ \tilde{r}^2 - \dfrac{\tilde{r}}{1+\tilde{r}^2}\right]^2 & r \text{ along } \hat{e}_n\end{cases} \tag{16}$$

for

$$a < r << \lambda$$

where

$$\tilde{r} = r/a.$$

Upon expanding the above expression in powers of $\tilde{r}^{-1}$ we find

$$\left(\frac{\bar{w}^{tr}}{\bar{w}^{inc}}\right)_{exact} \simeq \frac{8}{9\pi^2}\left(\frac{a}{r}\right)^6 \begin{cases}1[1 + 3\tilde{r}^{-2}/5 + O(\tilde{r}^{-4})] & r \text{ along } \hat{e}_{\|} \\ 4[1 + 6\tilde{r}^{-2}/5 + O(\tilde{r}^{-4})] & r \text{ along } \hat{e}_{\perp} \\ 1[1 - 12\tilde{r}^{-2}/5 + O(\tilde{r}^{-4})] & r \text{ along } \hat{e}_n\end{cases} \tag{17}$$

However, the first term of (17) corresponds to the approximate solution given in (15) which is based upon polarizabilities and identical to Bethe's result [1]. Explicitly, we find from (15),

$$\frac{\bar{w}^{tr}}{\bar{w}^{inc}} = \frac{8}{9\pi^2}\left(\frac{a}{r}\right)^6 \begin{cases}1 & r \text{ along } \hat{e}_{\|} \\ 4 & r \text{ along } \hat{e}_{\perp} \\ 1 & r \text{ along } \hat{e}_n\end{cases} \tag{18}$$

Thus, for $r << \lambda$, we expect the approximate solution outlined previously to hold for distances such that $r > a$. A comparison of the exact and approximate transmitted energy densities from equations (16) and (18)

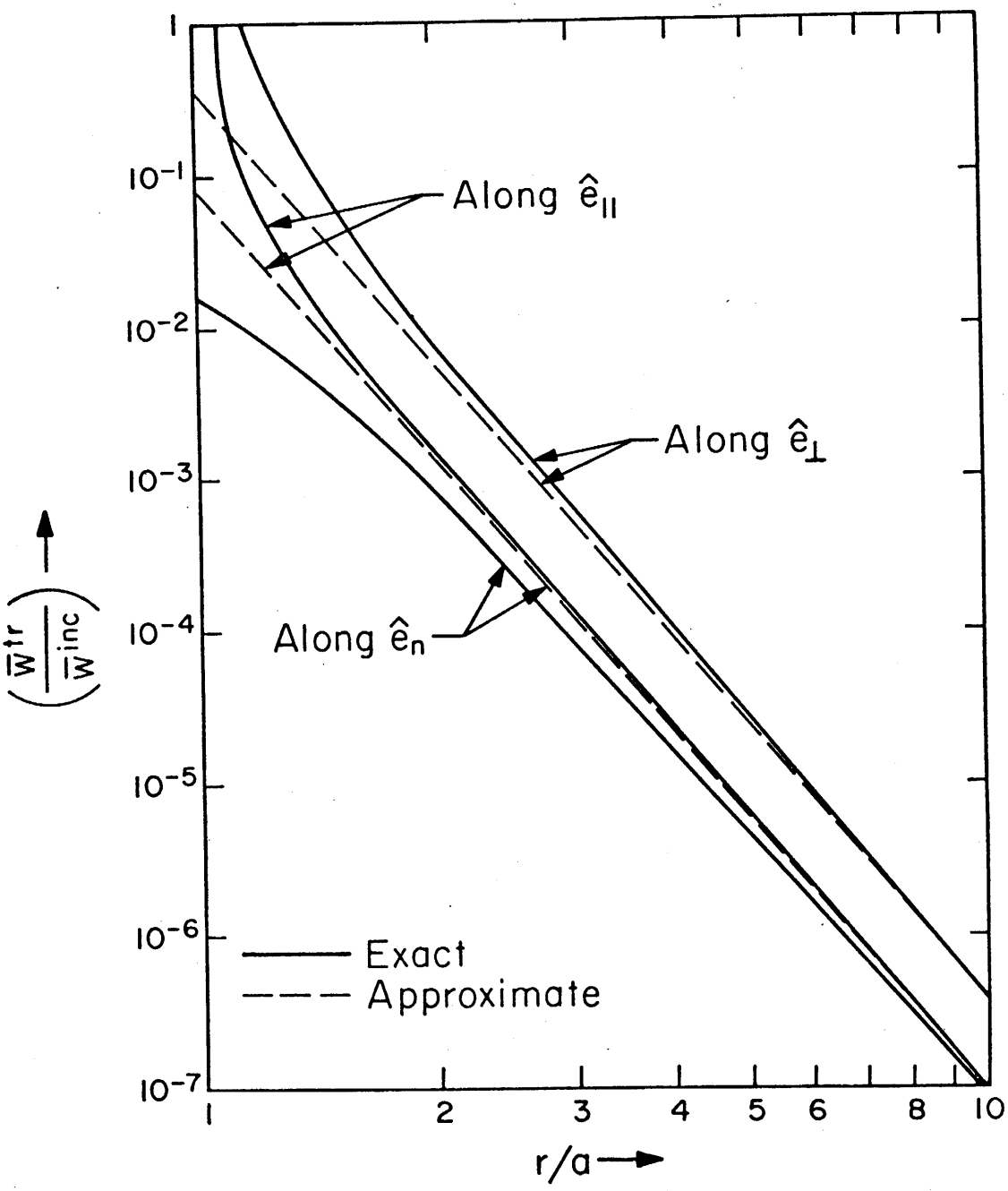

Figure 4. Ratio of Transmitted Energy Density to Incident Energy Density in the Near Field Along the Coordinate Axes. The exact expression is due to Bouwkamp and the approximate expression is the dipole approximation.

is shown in figure 4 as a function of normalized distance. It is clear from this figure that in the near field, the approximate solution based upon polarizabilities is adequate for observations at distances greater than or equal to the aperture diameter. The maximum error in the approximate expression for the energy density is less than 3% for $r/a \gtrsim 2$ with r taken along the $\hat{e}_{||}$ or $\hat{e}_{\perp}$ axes. Similar results hold for the calculation of individual field components.

The previous comparisons between exact and approximate values for the fields and energy transmitted through a small circular aperture were performed for the case of normal incidence. We assert that the results based upon polarizabilities can also be used for arbitrary polarizations and angles of incidence. This provides us with a means for calculating the near-field coupling among several small apertures regardless of the incident field orientation. Before carrying out the coupling calculations, several other computations will be made.

It is well known that the solution of Bethe is exact in the far-field (i.e., $r \gg \lambda$). Hence, we can use the previously developed equations (4-11) to find the distribution of transmitted energy.

$$\frac{\bar{w}^{tr}}{\bar{w}^{inc}} = \frac{16k^4a^6}{9\pi^2r^2} \begin{cases} \cos^2\beta[1 - \sin^2\theta \sin^2\phi] & \perp \text{ polarization} \\ [\cos^2\theta + \sin^2\theta(\cos^2\phi + \frac{1}{4}\sin^2\alpha) & \\ \quad + \sin\alpha \sin\theta \cos\phi] & || \text{ polarization} \end{cases} \tag{19}$$

for $r \gg \lambda$.

The transmitted energy density in this case is due to equal contributions from the electric and magnetic fields. Plots of the relative

distribution of the energy density are given in figure 5. We note the following facts concerning the far-field energy distribution:

1. maximum energy transmission occurs in a direction opposite to that of the incident wave vector for parallel polarization (this is similar to the large backscatter energy which occurs in scattering from an electrically small metallic sphere)
2. regardless of the angle of incidence, maximum energy transmission occurs in the direction normal to the aperture for perpendicular polarization (this is the usual dipole radiation which is similar to the scattering of energy from an electrically small dielectric sphere);
3. in all cases the far-field energy distribution is significantly different from the near-field distribution.

The transmission coefficient τ is defined as the ratio of the total far-field power transmitted through the aperture divided by the total power normally incident upon the aperture. This can be written as

$$\tau = \lim_{r \to \infty} \frac{\int_{RHS} \underline{E}^{tr} \times \underline{H}^{tr*} \cdot \hat{e}_r dA}{\int_{Ap} \underline{E}^{inc} \times \underline{H}^{inc*} \cdot \hat{e}_n dA} \tag{20}$$

where the integration is taken over the right-half-sphere in the numerator and over the aperture in the denominator. The result is

$$\tau = \frac{64}{27} \frac{(ka)^4}{\pi^2} \begin{cases} \cos\beta & \perp \text{ polarization} \\ \dfrac{1 + \frac{1}{4}\sin^2\alpha}{\cos\alpha} & \parallel \text{ polarization} \end{cases} \tag{21}$$

which agrees with well-known results for the circular aperture [1-3,10,11].

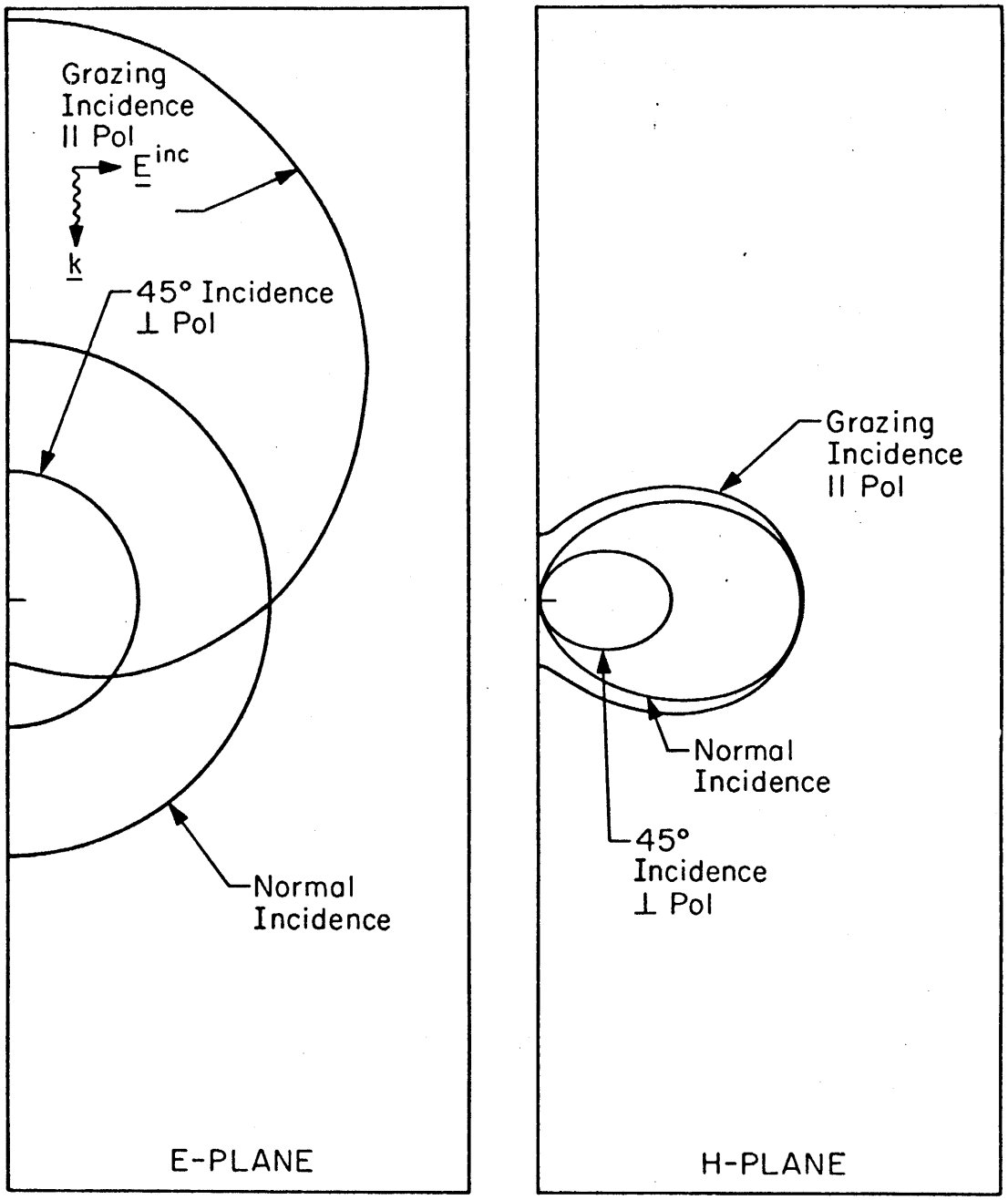

Figure 5. Relative Energy Distribution in the Far Field of a Small Circular Aperture. Note the maxima which occur in a direction opposite to that of the wave vector for grazing incidence.

SECTION III

NONCIRCULAR APERTURES

Noncircular apertures present additional computational difficulties for two reasons. First, the geometry prevents easy calculation of the magnetic and electric susceptibilities in most cases. Often numerical solutions are required. Second, the magnetic susceptibility becomes anisotropic. In this case the magnetic dipole moment is related to the magnetic field through a 2 by 2 matrix. As a result, magnetic dipoles appear along both the $\hat{e}_{||}$ and $\hat{e}_{\perp}$ axes while the electric dipole appears along the $\hat{e}_n$ axis as before.

In this section we first examine transmission through elliptical and rectangular apertures since many aperture geometries can be approximated by these shapes. We also make several comments and approximations regarding other aperture shapes. Our goal is to find simple expressions for the dipole moments or the transmission coefficient without resorting to the solution of complicated boundary-value problems.

The geometry for the problems considered is shown in figure 6. The triad of vectors $\underline{E}^{inc}/E^{inc}$, $\underline{H}^{inc}/H^{inc}$ and $\underline{k}/k$ are given by various rotations of the unit vector triad $\hat{e}_{||}$, $\hat{e}_{\perp}$ and $\hat{e}_n$. Consider a positive rotation about $\hat{e}_n$ by the angle χ which is followed by a negative rotation about $\hat{e}'_{\perp}$ ($\hat{e}'_{||}$) by α (β) for parallel (perpendicular) polarization. These operations produce the following relations.

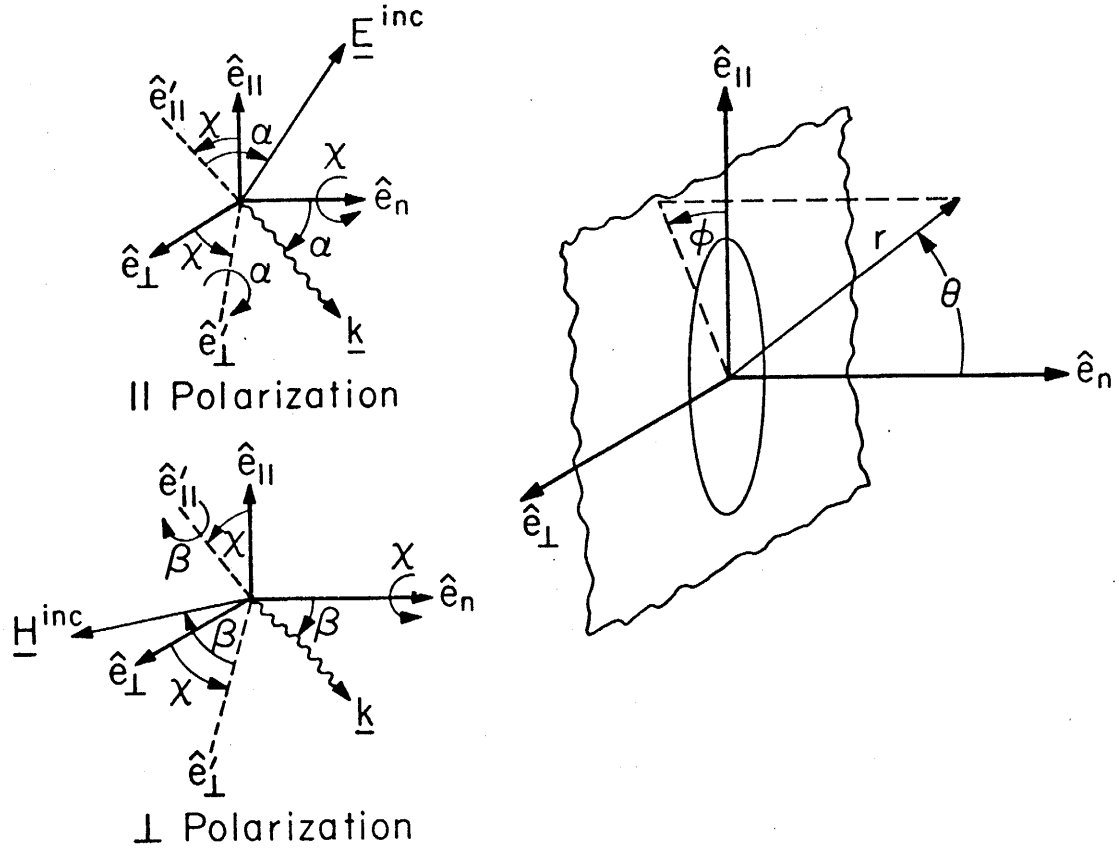

Figure 6. Geometry of Incident Fields and Noncircular Aperture for Parallel and Perpendicular Incidence.

$$\frac{\underline{k}}{k} = \begin{cases} -\sin\beta \sin\chi\, \hat{e}_{||} + \sin\beta \cos\chi\, \hat{e}_{\perp} + \cos\beta\, \hat{e}_n & \perp \text{ polarization} \\ -\sin\alpha \cos\chi\, \hat{e}_{||} - \sin\alpha \sin\chi\, \hat{e}_{\perp} + \cos\alpha\, \hat{e}_n & || \text{ polarization} \end{cases} \tag{22}$$

$$\frac{\underline{E}^{inc}}{E^{inc}} = \begin{cases} \cos\chi\, \hat{e}_{||} + \sin\chi\, \hat{e}_{\perp} & \perp \text{ polarization} \\ \cos\alpha \cos\chi\, \hat{e}_{||} + \cos\alpha \sin\chi\, \hat{e}_{\perp} + \sin\alpha\, \hat{e}_n & || \text{ polarization} \end{cases} \tag{23}$$

$$\frac{\underline{H}^{inc}}{H^{inc}} = \begin{cases} -\cos\beta \sin\chi\, \hat{e}_{||} + \cos\beta \cos\chi\, \hat{e}_{\perp} + \sin\beta\, \hat{e}_n & \perp \text{ polarization} \\ -\sin\chi\, \hat{e}_{||} + \cos\chi\, \hat{e}_{\perp} & || \text{ polarization} \end{cases} \tag{24}$$

For $\chi = 0$, the above incident fields are just those considered in the previous section (see figure 2). The projection of the magnetic field in the plane of the aperture is along the minor axis (see figures 6-7). For $\chi = \pi/2$, the projection of the magnetic field in the plane of the aperture is along the major axis (see figures 6-7).

We define the electric and magnetic dipole moments as

$$\underline{p}_e = \varepsilon_o\ \alpha_e\ (\underline{E}^{inc} \cdot \hat{e}_n)\ \hat{e}_n \tag{25}$$

$$\underline{p}_m^{(1)} = -\mu_o\, [\alpha_m^{(1)}\ (\underline{H}^{inc} \cdot \hat{e}_{||}) + \alpha_m^{(1,2)} (\underline{H}^{inc} \cdot \hat{e}_{\perp})]\ \hat{e}_{||} \tag{26}$$

$$\underline{p}_m^{(2)} = -\mu_o\, [\alpha_m^{(2)}\ (\underline{H}^{inc} \cdot \hat{e}_{\perp}) + \alpha_m^{(2,1)}\ (\underline{H}^{inc} \cdot \hat{e}_{||})]\ \hat{e}_{\perp} \tag{27}$$

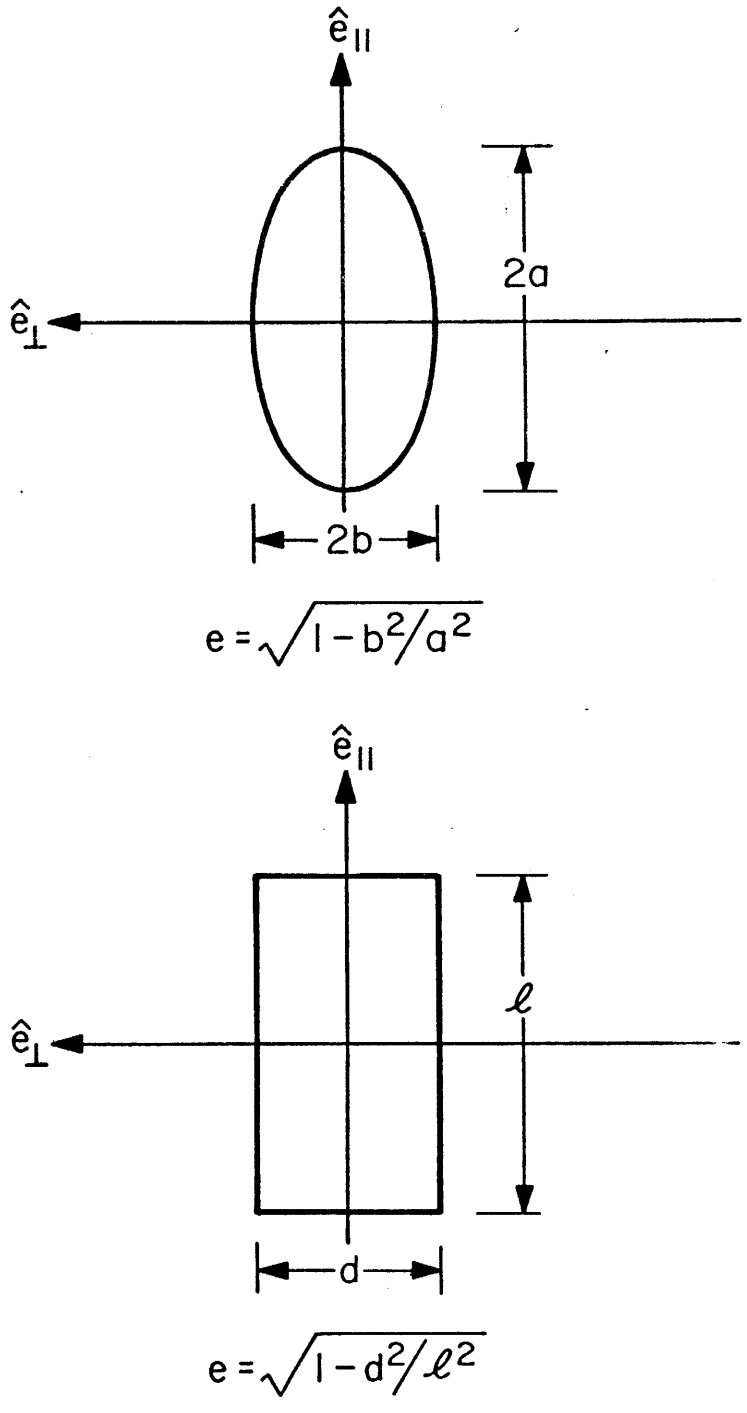

Figure 7. Geometry of the Aperture Plane for Elliptical and Rectangular Apertures. The eccentricities e are defined such that for $e = 0$ the ellipse becomes a circle and the rectangle becomes a square.

where α_e is the electric polarizability and $\alpha_m^{(1)}$, $\alpha_m^{(2)}$, $\alpha_m^{(1,2)}$ and $\alpha_m^{(2,1)}$ are the magnetic polarizabilities. The polarizabilities are dependent only upon geometric factors and are simply related to the susceptibilities introduced in the previous section. If lines of symmetry exist in the aperture, then $\alpha_m^{(1,2)} = \alpha_m^{(2,1)} = 0$ [12]. This will be the only case considered for the remainder of this section. Comparing equations (25-27) with (4-5) we find immediately that

$$(\alpha_e)_{circle} = \frac{8}{3} a^3 \tag{28}$$

$$(\alpha_m^{(1)})_{circle} = \frac{16}{3} a^3 \tag{29}$$

$$(\alpha_m^{(2)})_{circle} = \frac{16}{3} a^3 \tag{30}$$

A similar result for elliptical apertures with semiaxes a and b is well known [12,14] (see figure 7).

$$(\alpha_e)_{ellipse} = \frac{4\pi}{3} \frac{ab^2}{E(e^2)} \tag{31}$$

$$(\alpha_m^{(1)})_{ellipse} = \frac{4\pi}{3} \frac{ab^2e^2}{(1-e^2)[K(e^2) - E(e^2)]} \tag{32}$$

$$(\alpha_m^{(2)})_{ellipse} = \frac{4\pi}{3} \frac{ab^2e^2}{[E(e^2) - (1-e^2)\,K(e^2)]} \tag{33}$$

where

$$e = \sqrt{1 - b^2/a^2} = \text{eccentricity}$$

$$K(e^2) = \int_0^{\pi/2} \frac{d\theta'}{\sqrt{1-e^2 \sin^2\theta'}} = \text{complete elliptic integral of the first kind}$$

$$E(e^2) = \int_0^{\pi/2} \sqrt{1 - e^2 \sin^2\theta'}\, d\theta' = \text{complete elliptic integral of the second kind}$$

For future calculations we also write the expressions for the perimeter P and the area A (see figure 7).

$$(P)_{ellipse} = 4a\, E(e^2) = 4\sqrt{\frac{(A)_{ellipse}}{\pi}}\, \frac{E(e^2)}{(1-e^2)^{1/4}} \tag{34}$$

$$(A)_{ellipse} = \pi ab \tag{35}$$

The polarizabilities for the rectangular aperture are found by a numerical method [12]. The expressions for the perimeter and area are noted as

$$(P)_{rectangle} = 2(\ell+d) = 2\sqrt{(A)_{rectangle}}\, [(1-e^2)^{-1/4} + (1-e^2)^{1/4}] \tag{36}$$

$$(A)_{rectangle} = \ell d \tag{37}$$

where

$$e = \sqrt{1 - d^2/\ell^2} = \text{eccentricity}$$

for a rectangle of width d and length ℓ.

The normalized polarizabilities are plotted in figures 8 and 9 for elliptical and rectangular apertures of various eccentricities. We observe that for small eccentricities the polarizabilities are equal to the square of the area times a slowly varying function of eccentricity divided by the perimeter (i.e. $\alpha \simeq F(e)\ A^2/P$ where $F(e)$ is a slowly varying function of e). Thus, for small eccentricities, the polarizabilities are mainly dependent upon the ratio of the square of the area to the perimeter. This fact may indicate that simplified approximations to the polarizabilities can be made from simple geometric considerations.

Papas has asserted that the transmission coefficient τ for normal incidence and for apertures of any shape is bounded by simple expressions involving the area and perimeter of the aperture [7]. The simple expressions are found by substituting inner and outer radii, r_{in} and r_{out}, for the radius of a circle into the equation for τ given by (20-21). These radii are given by the expressions

$$\left.\begin{aligned} r_{in} &= \sqrt{\frac{A}{\pi}} \\ r_{out} &= \frac{P}{2\pi} \end{aligned}\right\} \qquad (38)$$

Application of the above equations to the values for the polarizabilities of a circle produce the following inequalities.

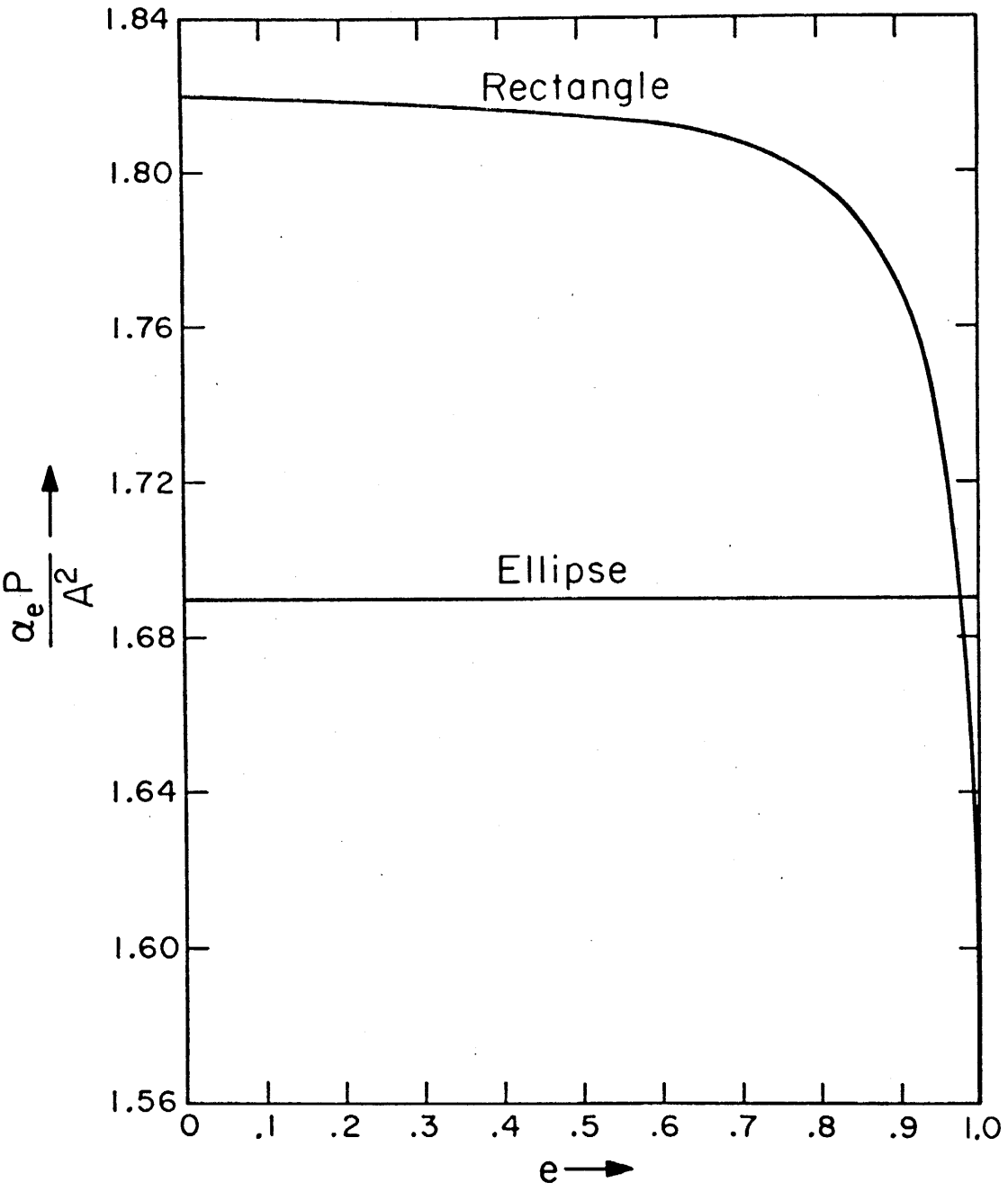

Figure 8. Normalized Electric Polarizability as a Function of Eccentricity.

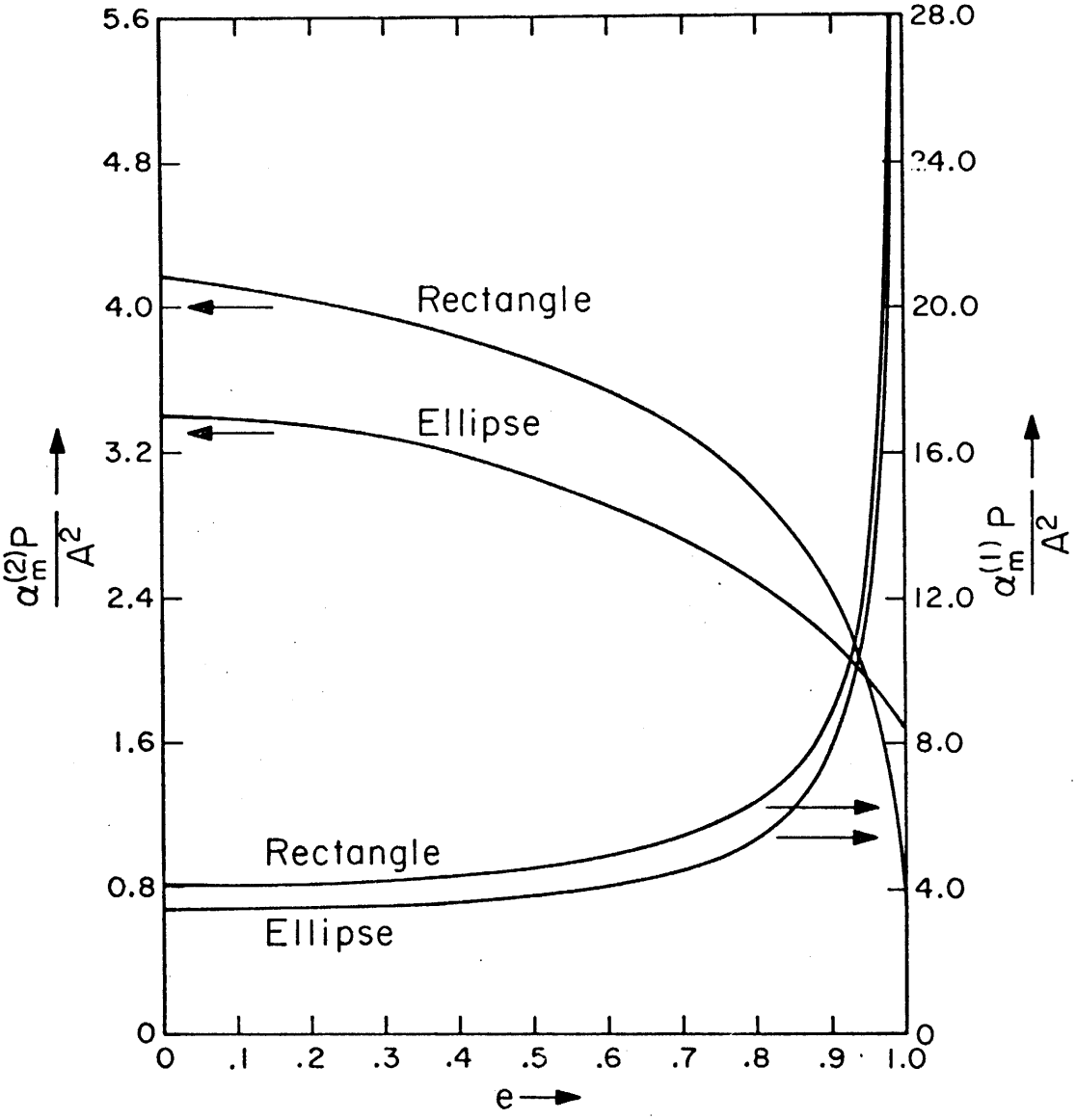

Figure 9. Normalized Magnetic Polarizability as a Function of Eccentricity.

$$\frac{8}{3}\left(\frac{A}{\pi}\right)^{3/2} \leq \alpha_e \leq \frac{8}{3}\left(\frac{P}{2\pi}\right)^{3} \tag{39}$$

$$\frac{16}{3}\left(\frac{A}{\pi}\right)^{3/2} \leq \alpha_m \leq \frac{16}{3}\left(\frac{P}{2\pi}\right)^{3} \tag{40}$$

However, a comparison of these inequalities with figures 8 and 9 or the expressions (31)-(33) show inconsistencies. For example, by applying (40) we find

$$\frac{8}{3}\left(\frac{A}{\pi}\right)^{3/2} \leq (\alpha_e)_{\text{ellipse}} \leq \frac{8}{3}\left(\frac{A}{\pi}\right)^{3/2}\left(1 + \frac{9}{64}e^4\right) \tag{41}$$

for $e \ll 1$

The actual value for the electric polarizability is given by

$$(\alpha_e)_{\text{ellipse}} = \frac{8}{3}\left(\frac{A}{\pi}\right)^{3/2}\left(1 - \frac{3}{64}e^4\right) \tag{42}$$

for $e \ll 1$

Therefore, the bounds in (39) are incorrect. In a similar manner, an examination of (40) shows discrepancies in the values for the magnetic polarizabilities since the bounds are given by

$$\frac{16}{3}\left(\frac{A}{\pi}\right)^{3/2} \leq (\alpha_m)_{\text{ellipse}} \leq \frac{16}{3}\left(\frac{A}{\pi}\right)^{3/2}\left(1 + \frac{9}{64}e^4\right) \tag{43}$$

for $e \ll 1$

whereas the actual values are

$$\begin{aligned}(\alpha_m^{(1)})_{\text{ellipse}} &= \frac{16}{3}\left(\frac{A}{\pi}\right)^{3/2}\left(1 + \frac{3}{8}e^2 + \frac{9}{32}e^4\right)\\ (\alpha_m^{(2)})_{\text{ellipse}} &= \frac{16}{3}\left(\frac{A}{\pi}\right)^{3/2}\left(1 - \frac{3}{8}e^2 - \frac{3}{32}e^4\right)\end{aligned} \tag{44}$$

for $e \ll 1$

Since these bounds are based on scalar calculations rather than vector calculations, it is not surprising that the calculation may fail when polarization is important (i.e., for calculations of $\alpha_m^{(1)}$ and $\alpha_m^{(2)}$. However, for incoherent or randomly polarized incident fields the arithmetic of the magnetic polarizabilities (i.e., one-half of the trace of the 2x2 matrix) should be the important quantity. This quantity is invariant under axis rotations and is given by the definition

$$\langle \alpha_m \rangle = \frac{\alpha_m^{(1)} + \alpha_m^{(2)}}{2} \tag{45}$$

For the ellipse

$$\langle \alpha_m \rangle_{\text{ellipse}} = \frac{16}{3} \left(\frac{A}{\pi}\right)^{3/2} \left(1 + \frac{3}{32} e^4\right) \tag{46}$$

for $e << 1$

which does satisfy the bounds of equation (43). A further numerical comparison for the elliptical and rectangular aperture shows that the mean magnetic polarizability satisfies the bounds of (40) for all eccentricities (see appendix). This is not surprising, since both the cube of the perimeter and the largest polarizability vary as $(1 - e^2)^{-3/4}$ for large eccentricities. These bounds indicate that for an aperture of given area the magnetic polarizability is smallest for the circular aperture.

A fix-up may also be found for the electric polarizability. Noting that this quantity varies as A^2/P, we can rewrite the expression for the electric polarizability as $8A^2/3\pi^2 a$ for a circular aperture of radius a. Replacing the radius by the outer and inner radii respectively, we calculate the upper and lower bounds for an aperture of arbitrary shape

$$\frac{16}{3\pi} \frac{A^2}{P} \leq \alpha_e \leq \frac{8}{3} \left(\frac{A}{\pi}\right)^{3/2} \tag{47}$$

For the ellipse this becomes

$$\frac{8}{3}\left(\frac{A}{\pi}\right)^{3/2}\left(1-\frac{3}{64}e^4\right) \leq (\alpha_e)_{\text{ellipse}} \leq \frac{8}{3}\left(\frac{A}{\pi}\right)^{3/2} \qquad (48)$$

for $e \ll 1$

which is satisfied by (42). The bounds indicate that for an aperture of given area, the circular aperture has the largest electric polarizability. We note that the bounds are sufficient for elliptical and rhombical apertures but that the lower bound breaks down for rectangular apertures of large eccentricity (see appendix and Ref. [12]). For long narrow rectangular slits the lower bound overestimates the electric polarizability by approximately 8%.

The following list summarizes the findings concerning polarizabilities:

1. We assert that the following bounds hold for convex apertures with small eccentricities

$$\frac{16}{3\pi}\frac{A^2}{P} \leq \alpha_e \leq \frac{8}{3}\left(\frac{A}{\pi}\right)^{3/2}$$

$$\frac{16}{3}\left(\frac{A}{\pi}\right)^{3/2} \leq \langle\alpha_m\rangle \leq \frac{16}{3}\left(\frac{P}{2\pi}\right)^3 \qquad (49)$$

2. The lower bound given by (49) approximates the electric polarizability for small eccentricities, but may slightly overestimate this quantity for large eccentricities;
3. The upper bound given by (49) approximates the larger magnetic polarizability but underestimates this value;
4. The circular aperture will produce the smallest maximum transmitted field of any convex aperture of a given area, since the ratio of perimeter to area is the smallest for this shape [7].

Additional tables of polarizabilities and related quantities are given in the appendix.

To show explicitly the usefulness of the previous results, it is necessary to find the transmitted fields that are due to the dipole sources $\underline{p}_e$, $\underline{p}_m^{(1)}$ and $\underline{p}_m^{(2)}$. From Papas [9] we write

$$E_r^{tr} = \frac{1}{\varepsilon_o} p_e \cos\theta \left(\frac{-2ik}{r} + \frac{2}{r^2}\right)G \tag{50}$$

$$E_\theta^{tr} = -\frac{1}{\varepsilon_o} p_e \sin\theta \left(\frac{ik}{r} - \frac{1}{r^2} + k^2\right)G + i\omega\left(p_m^{(1)} \sin\phi - p_m^{(2)} \cos\phi\right) \cdot \left(ik - \frac{1}{r}\right)G \tag{51}$$

$$E_\phi^{tr} = i\omega\left(p_m^{(1)}\cos\phi + p_m^{(2)}\sin\phi\right) \cos\theta\left(ik - \frac{1}{r}\right)G \tag{52}$$

$$H_r^{tr} = \frac{1}{\mu_o}\left(p_m^{(1)}\cos\phi + p_m^{(2)}\sin\phi\right) \sin\theta\left(\frac{-2ik}{r} + \frac{2}{r^2}\right)G \tag{53}$$

$$H_\theta^{tr} = \frac{1}{\mu_o}\left(p_m^{(1)}\cos\phi + p_m^{(2)}\sin\phi\right) \cos\theta\left(\frac{ik}{r} - \frac{1}{r^2} + k^2\right)G \tag{54}$$

$$H_\phi^{tr} = i\omega p_e \sin\theta\left(ik - \frac{1}{r}\right)G - \frac{1}{\mu_o}\left(p_m^{(1)}\sin\phi - p_m^{(2)}\cos\phi\right) \cdot \left(\frac{ik}{r} - \frac{1}{r^2} + k^2\right)G \tag{55}$$

where $G = e^{ikr}/4\pi r$, and where the time dependent $e^{-i\omega t}$ has again been suppressed. The distribution of energy for the above expressions is given by the ratio of the transmitted energy density to the incident energy density. This expression in the far field is

$$\frac{\bar{w}^{tr}}{\bar{w}^{inc}} = \frac{k^4}{16\pi r^2} \left\{ [\alpha_e^2 \sin^2\alpha \sin^2\theta + 2\alpha_e \sin\alpha \sin\theta \cdot (\alpha_m^{(1)} \sin\chi \sin\phi + \alpha_m^{(2)} \cos\chi \cos\phi)] \begin{pmatrix} 0 \\ 1 \end{pmatrix} \right.$$

$$+ [\alpha_m^{(1)2} \sin^2\chi (1 - \cos^2\phi \sin^2\theta) + \alpha_m^{(2)2} \cos^2\chi (1 - \sin^2\phi \sin^2\theta)$$

$$\left. + 2\alpha_m^{(1)} \alpha_m^{(2)} \sin\chi \cos\chi \sin\phi \cos\phi \sin^2\theta] \begin{pmatrix} \cos^2\beta \\ 1 \end{pmatrix} \right\} \qquad (56)$$

for $\begin{pmatrix} \perp \\ \parallel \end{pmatrix}$ polarization and $r >> \lambda$.

For the cases where the projection of the magnetic field on the plane of the screen is along the major ($\chi = \pi/2$) or minor ($\chi = 0$) axis of the aperture, we have the following simplifications:

$$\frac{w^{tr}}{w^{inc}} = \frac{k^4}{16\pi r^2} \left[(\alpha_e^2 \sin^2\alpha \sin^2\theta + 2\alpha_e \alpha_m^{(1)} \sin\alpha \sin\phi \sin\theta) \begin{pmatrix} 0 \\ 1 \end{pmatrix} \right.$$

$$\left. + \alpha_m^{(1)2} (1 - \cos^2\phi \sin^2\theta) \begin{pmatrix} \cos^2\beta \\ 1 \end{pmatrix} \right] \qquad (57)$$

for $\chi = \pi/2$,

$$\frac{w^{tr}}{w^{inc}} = \frac{k^4}{16\pi r^2} \left[(\alpha_e^2 \sin^2\alpha \sin^2\theta + 2\alpha_e \alpha_m^{(2)} \sin\alpha \cos\phi \sin\theta) \begin{pmatrix} 0 \\ 1 \end{pmatrix} \right.$$

$$\left. + \alpha_m^{(2)2} (1 - \sin^2\phi \sin^2\theta) \begin{pmatrix} \cos^2\beta \\ 1 \end{pmatrix} \right] \qquad (58)$$

for $\chi = 0$ and $\begin{pmatrix} \perp \\ \parallel \end{pmatrix}$ polarization.

The last expression is identical to equation (19) which was found before for the circular aperture. Several plots of the transmitted energy through an elliptical aperture are shown in figures 10 and 11 for normal

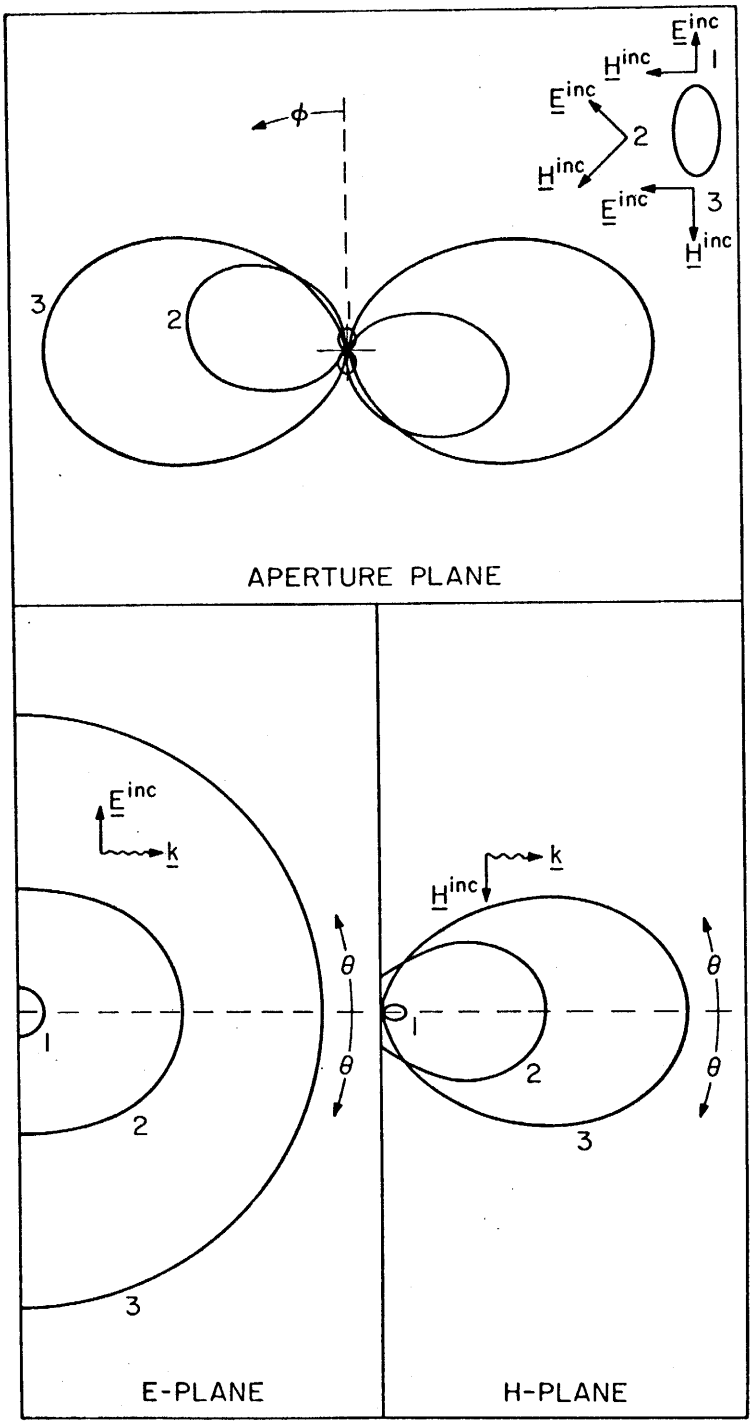

Figure 10. Relative Energy Distribution in the Far Field for a Small Elliptical Aperture of Eccentricity e = 0.9. The incident wave is normally incident.

and grazing (parallel polarization) incidence. Three incident field orientations are considered in each of these figures. The eccentricity is 0.9. Here the E-plane is defined by $\underline{E}^{inc}$ and $\hat{e}_n$ (or $\underline{E}^{inc}$ and $\underline{k}$ for grazing incidence), and the H-plane is defined by $\underline{H}^{inc}$ and $\hat{e}_n$. As expected, the transmitted energy is increased as the magnetic field becomes aligned with the major axis of the ellipse. The asymmetries evidenced in figure 11 are due to the interference between the various dipole moments. We again note the large backscatter which is particularly evidenced in figure 11. Here the maximum energy transmission is in a direction opposite to that of the incident wave vector. This phenomenon cannot be accounted for by Kirchhoff diffraction theory, but is typical of problems involving scattering from electrically small metallic particles.

The transmission coefficient is

$$\tau = \frac{k^4}{12\pi A} \frac{\alpha_e^2 \sin^2\gamma \begin{pmatrix} 0 \\ 1 \end{pmatrix} + (\alpha_m(1)^2 \sin^2\chi + \alpha_m(2)^2 \cos^2\chi) \begin{pmatrix} \cos^2\gamma \\ 1 \end{pmatrix}}{\cos\gamma} \tag{59}$$

for $\begin{pmatrix} \perp \\ \parallel \end{pmatrix}$ polarization, where $\cos\gamma = \underline{k}\cdot\hat{e}_n/k$ and A = aperture area.

We can place bounds on the maximum transmission by considering the inequality given by (49). By taking the maximum value of the square of this quantity we find

$$\left.\begin{aligned} \alpha_m(1)^2 \text{ or } \alpha_m(2)^2 &\leq 4\left[\frac{16}{3}\left(\frac{P}{2\pi}\right)^3\right]^2 \\ \alpha_e^2 &\leq \left[\frac{8}{3}\left(\frac{A}{\pi}\right)^{3/2}\right]^2 \leq \left[\frac{8}{3}\left(\frac{P}{2\pi}\right)^3\right]^2 \end{aligned}\right\} \tag{60}$$

This produces an absolute upper bound for the square of the polarizabilities and hence produces an upper bound for the transmission coefficient. However, under this approximation, which holds for large eccentricies, the smaller magnetic polarizability is negliglble when compared with the

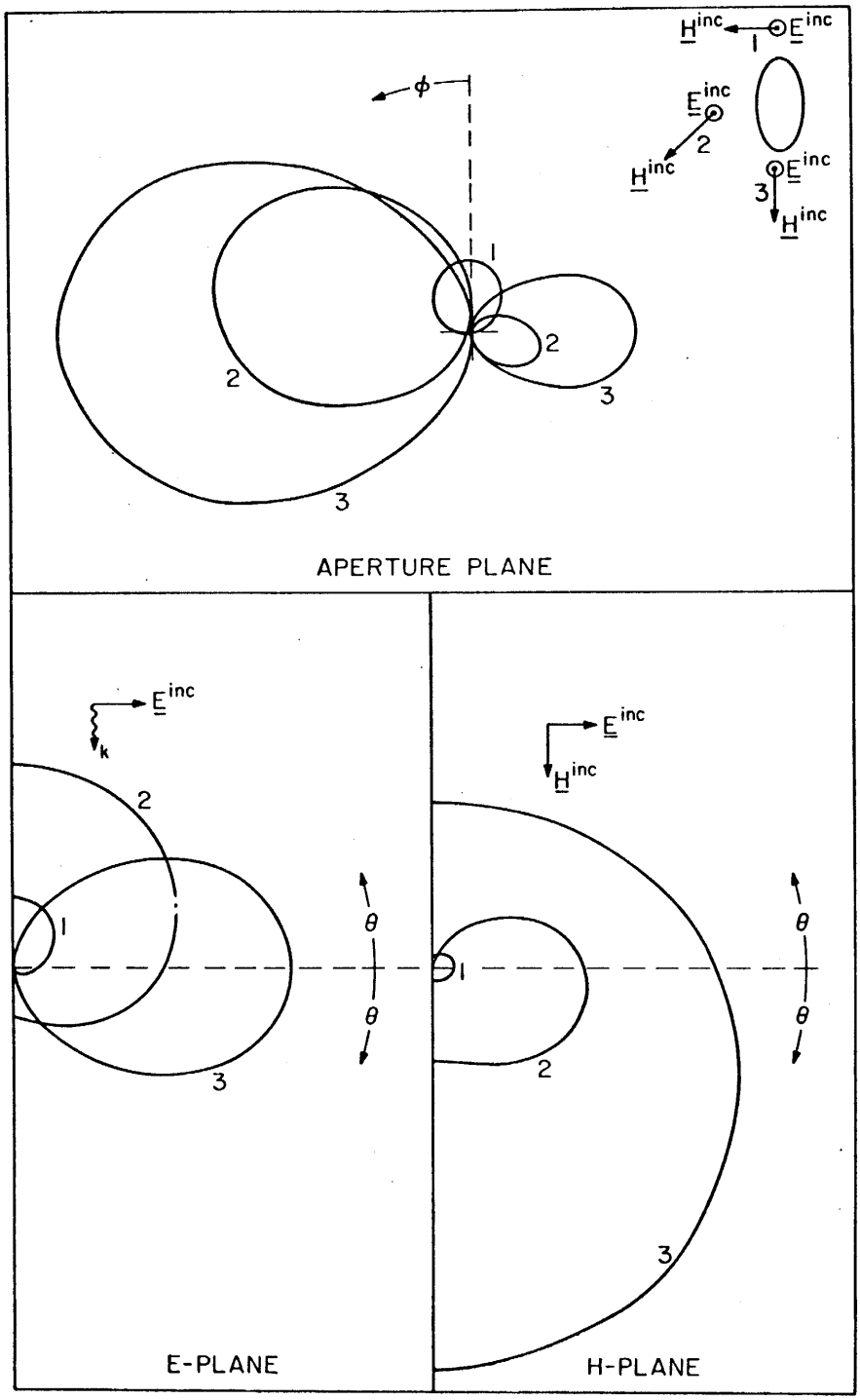

Figure 11. Relative Energy Distribution in the Far Field for a Small Elliptical Aperture of Eccentricity e = 0.9. The incident wave is grazing the aperture plane.

larger polarizability. Hence, the use of one-half of the value given by the upper value of expression (60) is suggested when the transmission coefficient is calculated. This suggestion is further supported if we remember that the upper bound of the mean magnetic polarizability also approximates the largest polarizability. For small eccentricities we use the polarizabilities which are given for the circular aperture. Thus we have the following approximation for the maximum transmission coefficient

$$\tau_{Approx} = \frac{k^4}{12\pi A}\left[\frac{\frac{1}{4}\sin^2\gamma\binom{0}{1} + 2\binom{\cos^2\gamma}{1}}{\cos\gamma}\right]\begin{cases}\left[\frac{16}{3}\left(\frac{P}{2\pi}\right)^3\right]^2 & e \to 1 \\ \left[\frac{16}{3}\left(\frac{A}{\pi}\right)^{3/2}\right]^2 & e \ll 1\end{cases} \qquad (61)$$

for $\binom{\perp}{\parallel}$ polarization.

Plots of the exact expression (59) and the approximation (61) are given in figure 12 for an elliptical aperture and a variety of incident field orientations. It is apparent that the approximations give appropriate bounds on the maximum transmission (i.e., for $\chi = \pi/2$), but they may not be very useful for calculations involving intermediate eccentricities. The absolute upper bound for the transmission is found by multiplying the second term in the upper expression of (61) by the numerical factor 2.

A more useful approximation is found for the transmission coefficient of unpolarized waves. Averaging equation (59) over input polarizations and summing over output polarizations we find that

$$\langle\tau\rangle = \frac{k^4}{48\pi A}\left[\frac{\alpha_e^2\sin^2\gamma + (\alpha_m(1)^2 + \alpha_m(2)^2)(1+\cos^2\gamma)}{\cos\gamma}\right] \qquad (62)$$

By using the same approximations as in (61) we find

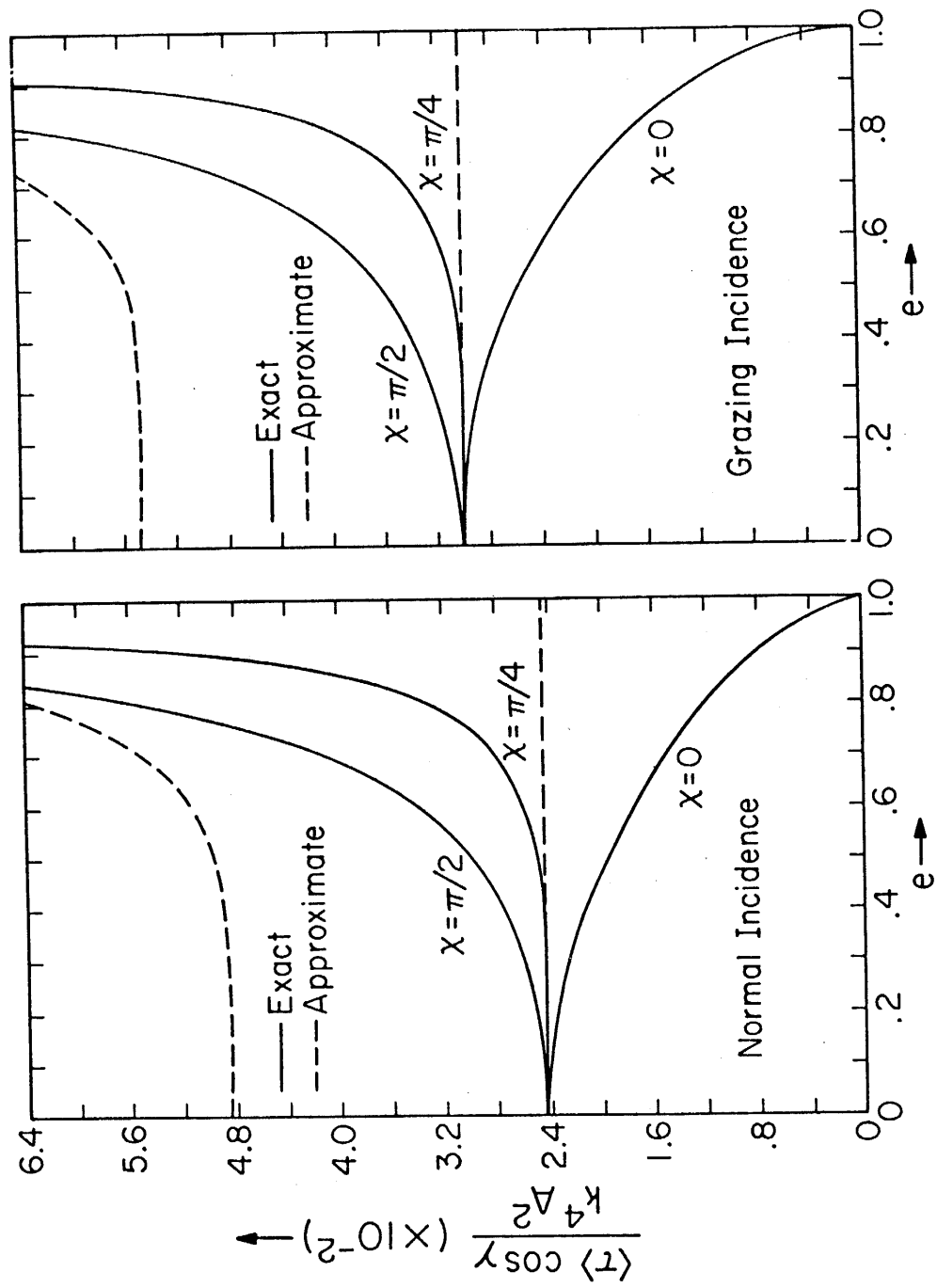

Figure 12. Transmission Coefficient of an Elliptical Aperture for Polarized Incident Fields. The values $\chi = 0$, $\pi/4$, $\pi/2$ correspond to the numbers 1, 2, 3 in figures 10 - 11.

$$\langle\tau\rangle_{\text{Approx}} = \frac{k^4}{48\pi A}\left[\frac{\frac{1}{4}\sin^2\gamma + 2\,(1+\cos^2\gamma)}{\cos\gamma}\right]\begin{cases}\left[\frac{16}{3}\left(\frac{P}{2\pi}\right)^3\right]^2 & e \to 1\\ \left[\frac{16}{3}\left(\frac{A}{\pi}\right)^{3/2}\right]^2 & e \ll 1\end{cases} \qquad (63)$$

The plots of equations (62) and (63) are given in figure 13 for an elliptical aperture. Note that maximum transmission occurs for normal incidence and that the approximation is accurate to within a few percent of the exact expression. The approximation is very good in this case because the polarization effects are averaged out and the vector nature of the problem becomes less important. An absolute upper-bound for the transmission is given when the second term of the upper expression in (63) is multiplied by the numerical factor 2. However, this absolute bound is not very useful for calculations since it is significantly larger than the actual value. We assert that the approximation given by (62) is good for other shapes as well. For example, in figure 14 we show how eccentricities can be defined for the isosceles triangle and the rhombus. The relations between the area, perimeter and eccentricity for these figures are given in the appendix. Plots of the maximum transmission (i.e., for normal incidence) as a function of eccentricity are shown in figure 15 for unpolarized waves. The values are derived from equation (63). Note the sharp increase in energy transmission for $e \gtrsim 0.7$.

We assert that for any given area and eccentricity, the ordering of shapes as a function of increasing transmission is as follows: ellipse, rectangle, rhombus and isosceles triangle. This ordering is identical to the ordering of the ratios of perimeter to area for each shape. This assertion on ordering is supported by the experimental polarizability measurements of Cohn [15,16].

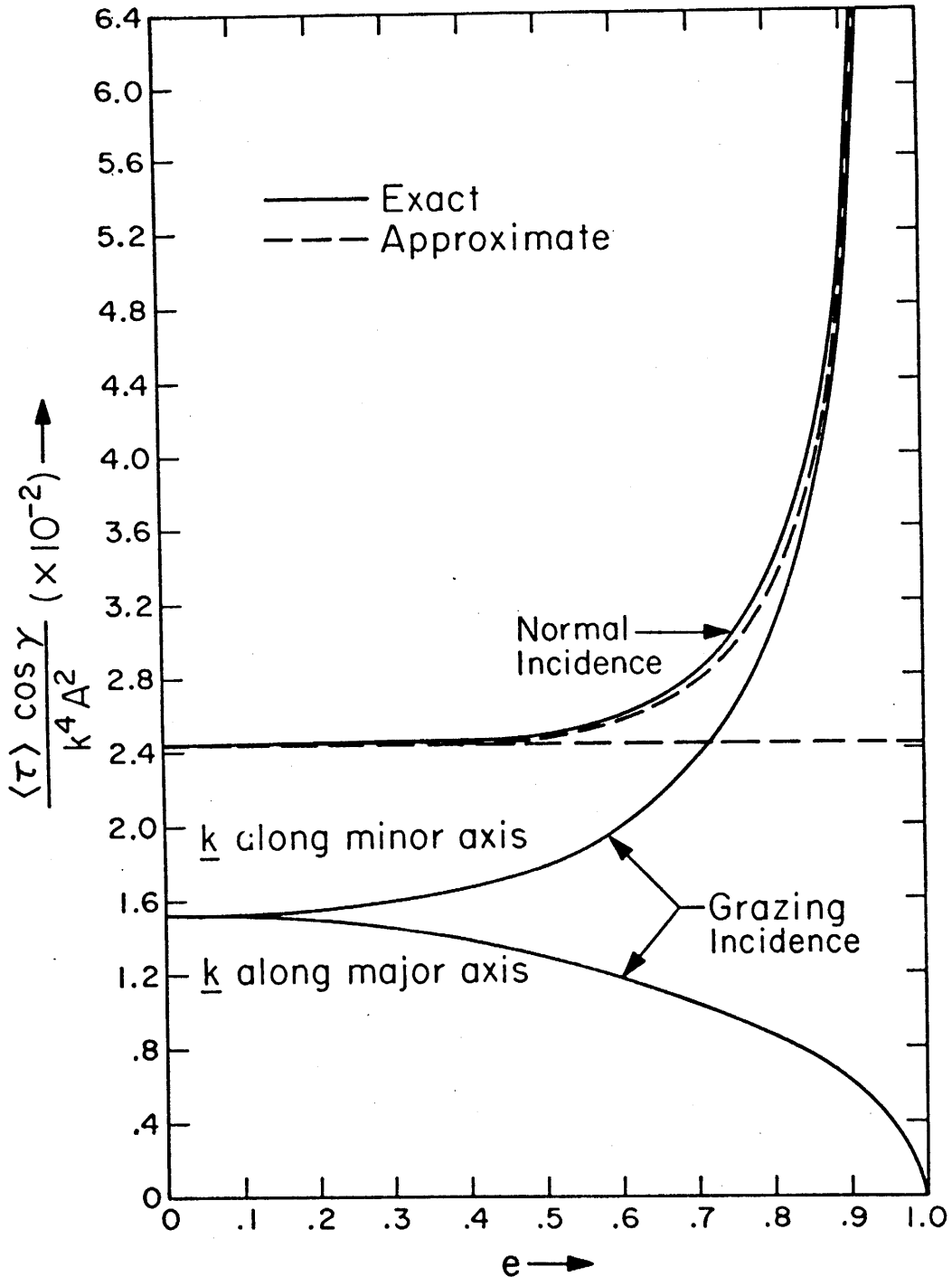

Figure 13. Transmission Coefficient of an Elliptical Aperture for Unpolarized Incident Fields.

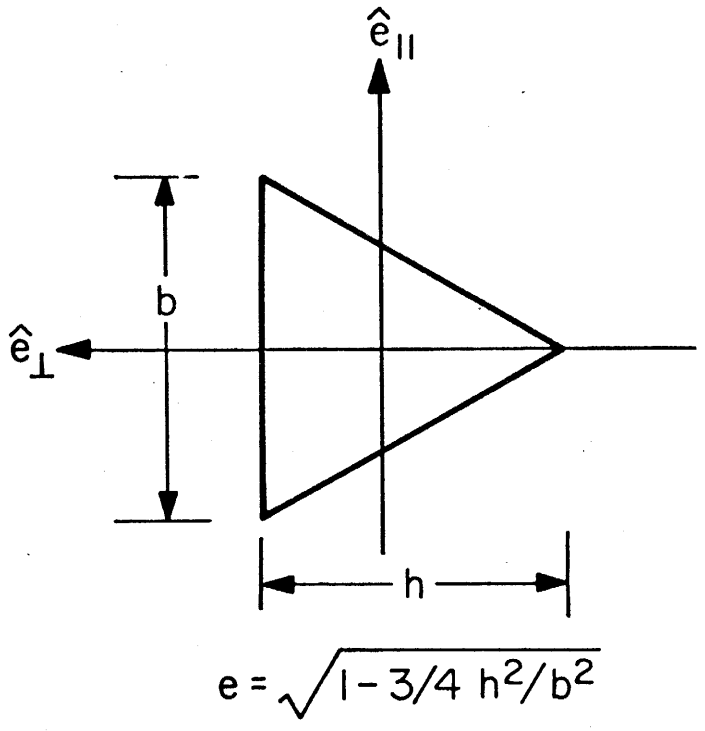

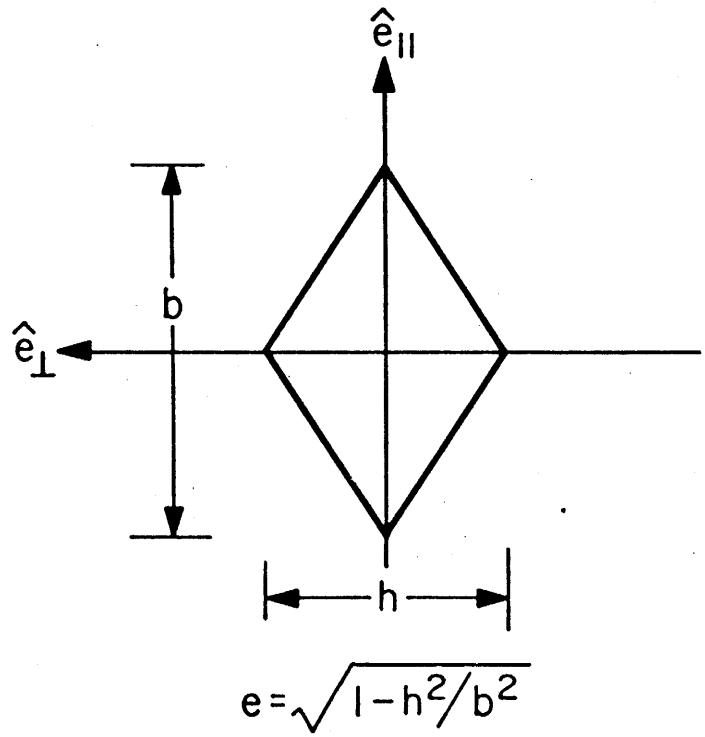

Figure 14. Geometry of the Aperture Plane for Triangular and Rhombical Apertures. The eccentricities e are defined so that for e = 0 , the isoceles triangle and rhombus became an equilateral triangle and a square.

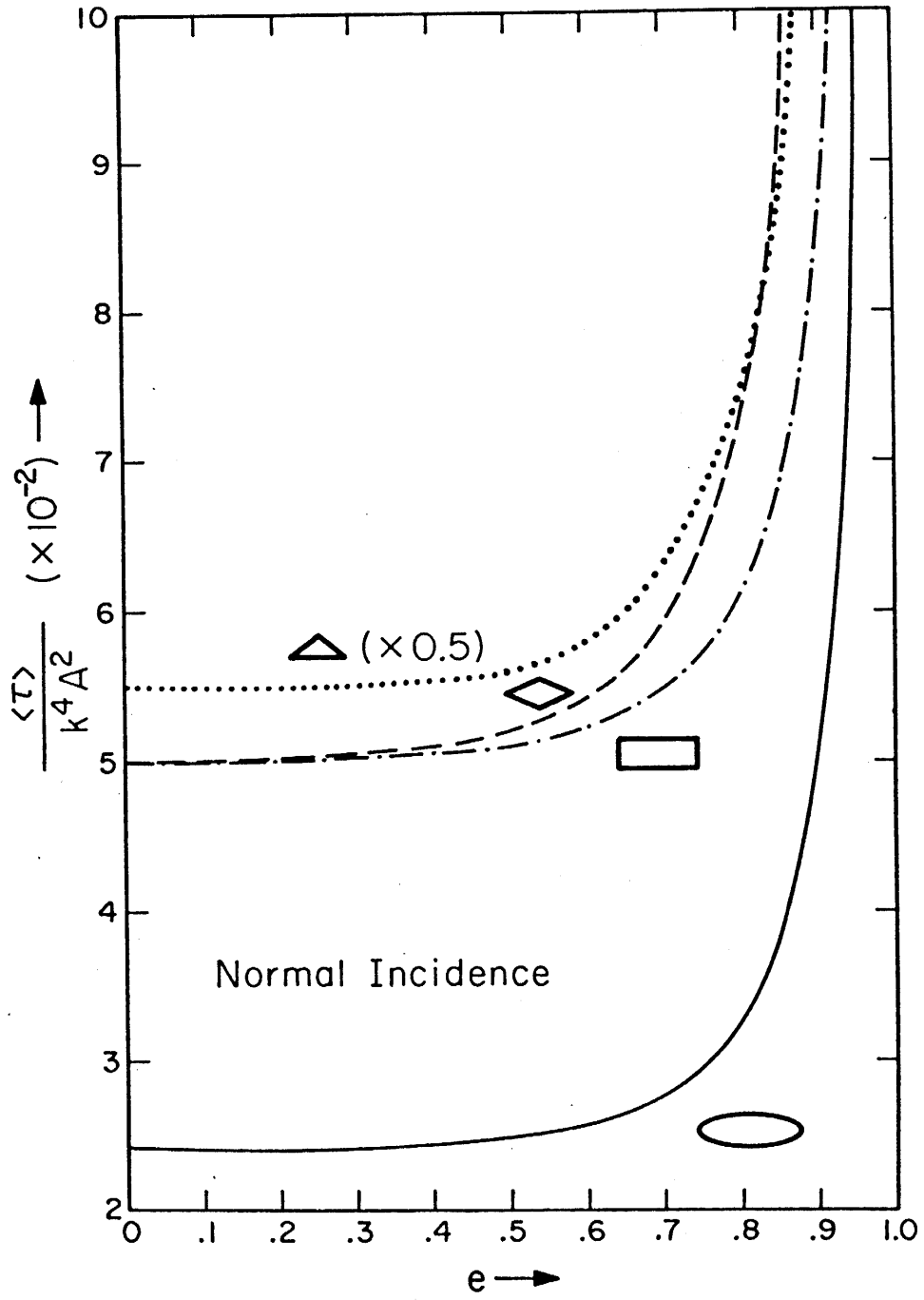

Figure 15. Approximate Value for the Transmission Coefficient of Various Shaped Apertures with Unpolarized Incident Fields.

In this section we have examined several types of convex non-circular apertures, of which the elliptical aperture is the archetype. Expressions and plots of the energy distribution are given. The use of equivalent radii provide upper and lower bounds on the maximum polarizabilities and transmission coefficients and provide approximate values for these quantities. Further work must be done to find more accurate bounds and approximations for polarized waves. However, very accurate approximations are found for the unpolarized case. Based on these approximations, we assert that the ordering of differently shaped apertures of equal area as a function of increasing transmission can be made by simply ordering the perimeters. Tables of values corresponding to some of the figure values are given in the appendix.

SECTION IV

COUPLING BETWEEN TWO APERTURES

Two apertures which are in close electrical proximity will interact through the coupling of electromagnetic fields. For example, the scattered field of the first aperture will impinge upon the second aperture. Therefore, the second aperture will be excited by the vectorial sum of both the scattered field of the first aperture and the incident field. Similar coupling occurs in the theory of artificial dielectrics [8,14].

The geometry for the two apertures under consideration is shown in figure 16. The notation for the incident fields is identical to that of the previous section (equations [22 - 24]). The line connecting the two apertures makes an angle ψ with respect to $\hat{e}_{||}$ and the apertures are separated by a distance d. The important coupling fields will be the near fields. All other fields will be a factor kd smaller, and we assume initially that $kd << 1$. It can be shown that at distances where the intermediate and far fields become comparable to the near field, the coupling becomes negligible. Thus, we will use the near-field or static approximation for coupling calculations.

The calculation starts by including interaction fields $\underline{E}^{int}$ and $\underline{H}^{int}$ in addition to the incident fields $\underline{E}^{inc}$ and $\underline{H}^{inc}$ in the calculation for the dipole moments.

$$p_e = \varepsilon_o \alpha_e [(\underline{E}^{inc} + \underline{E}^{int}/2) \cdot \hat{e}_n]\hat{e}_n \tag{64}$$

$$p_m^{(1)} = -\mu_o [\alpha_m^{(1)} (\underline{H}^{inc} + \underline{H}^{int}/2) \cdot \hat{e}_{||} + \alpha_m^{(1,2)} (\underline{H}^{inc} + \underline{H}^{int}/2) \cdot \hat{e}_{\perp}]\hat{e}_{||} \tag{65}$$

$$p_m^{(2)} = -\mu_o [\alpha_m^{(2)} (\underline{H}^{inc} + \underline{H}^{int}/2) \cdot \hat{e}_{\perp} + \alpha_m^{(2,1)} (\underline{H}^{inc} + \underline{H}^{int}/2) \cdot \hat{e}_{||}]\hat{e}_{\perp} \tag{66}$$

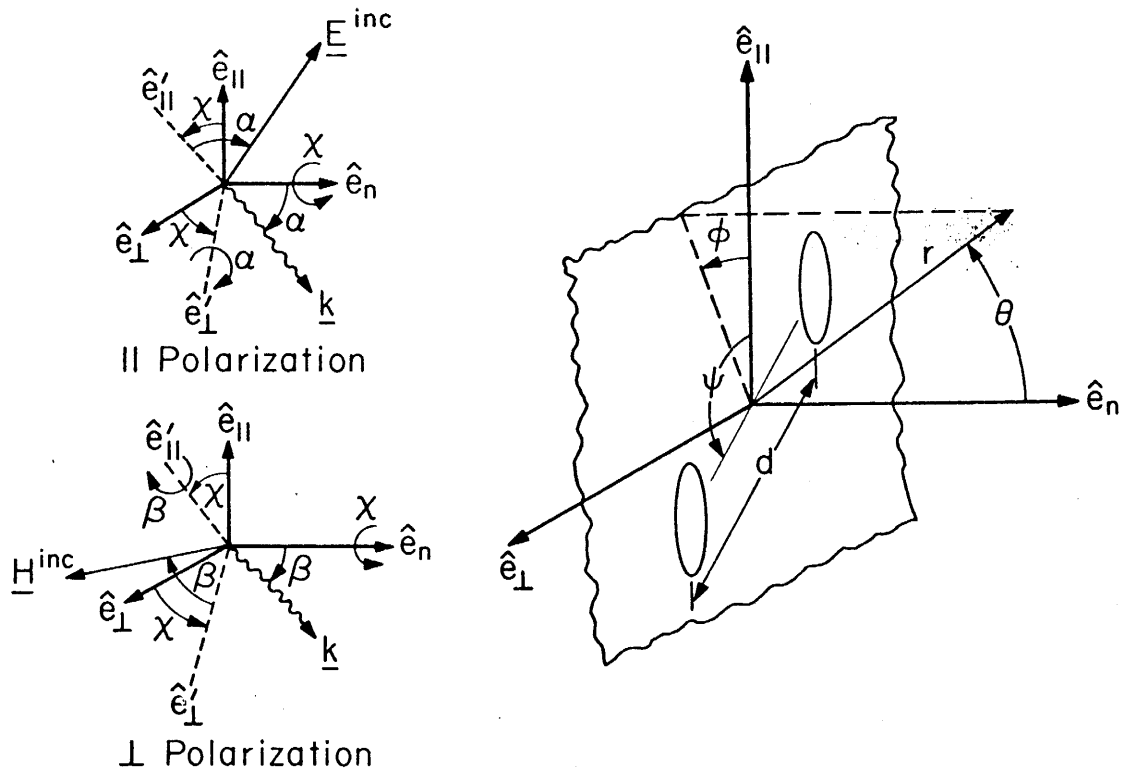

Figure 16. Geometry of Incident Fields and Two Noncircular Apertures for Parallel and Perpendicular Polarization.

The interaction fields are simply the scattered fields of the other aperture. (The factor of 1/2 appears in the interaction field terms since the polarizabilities are defined for this report in terms of one-half the total field at the aperture.) In the static approximation we find the dominant interaction fields in the aperture plane on the illuminated side. These fields are opposite in sign to the fields on the shadow side. We calculate

$$E_n^{int} = \frac{p_e}{2\pi\epsilon_o d^3} \tag{67}$$

$$H_{||}^{int} = -\frac{p_m^{(1)}(3\cos^2\psi - 1) + p_m^{(2)}\, 3\sin\psi\cos\psi}{2\pi\mu_o d^3} \tag{68}$$

$$H_{\perp}^{int} = -\frac{p_m^{(2)}(3\sin^2\psi - 1) + p_m^{(1)}\, 3\sin\psi\cos\psi}{2\pi\mu_o d^3} \tag{69}$$

(where magnetic [electric] interaction fields have been ignored due to electric [magnetic] dipole moments). By substituting equations (67-69) into (64-66) we can find equivalent polarizabilities $\tilde{\alpha}_e$, $\tilde{\alpha}_m^{(1)}$ and $\tilde{\alpha}_m^{(2)}$ which relate the dipole moments directly to the incident fields. By assuming that the total interaction is small (i.e., $d \gtrsim 1.5L$ where L is a typical aperture dimension) and keeping only the first power of polarizability/(separation)^3 we find after some algebraic manipulation

$$\underline{p}_e = \epsilon_o \tilde{\alpha}_e [\underline{E}^{inc} \cdot \hat{e}_n]\, \hat{e}_n \tag{70}$$

$$\underline{p}_m^{(1)} = -\mu_o [\tilde{\alpha}_m^{(1)}(\underline{H}^{inc} \cdot \hat{e}_{||}) + \tilde{\alpha}_m^{(1,2)}(\underline{H}^{inc} \cdot \hat{e}_{\perp})]\, \hat{e}_{||} \tag{71}$$

$$\underline{p}_m^{(2)} = -\mu_o[\tilde{\alpha}_m^{(2)}(\underline{H}^{inc}\cdot \hat{e}_\perp) + \tilde{\alpha}_m^{(2,1)}(\underline{H}^{inc}\cdot \hat{e}_{||})]\,\hat{e}_\perp \tag{72}$$

where

$$\tilde{\alpha}_e \simeq \alpha_e\left[1 - \frac{\alpha_e}{4\pi d^3}\right]^{-1} \tag{73}$$

$$\tilde{\alpha}_m^{(1)} \simeq \alpha_m^{(1)}\left[1 - \frac{\alpha_m^{(1)}(3\cos^2\psi - 1) + \alpha_m^{(1,2)}3\sin\psi\cos\psi}{4\pi d^3}\right]^{-1}$$

$$+ \alpha_m^{(2,1)}\left[\frac{\alpha_m^{(1,2)}(3\sin^2\psi - 1) + \alpha_m^{(1)}3\sin\psi\cos\psi}{4\pi d^3}\right] \tag{74}$$

$$\tilde{\alpha}_m^{(2)} \simeq \alpha_m^{(2)}\left[1 - \frac{\alpha_m^{(2)}(3\sin^2\psi - 1) + (\alpha_m^{(2,1)}3\sin\psi\cos\psi}{4\pi d^3}\right]^{-1}$$

$$+ \alpha_m^{(1,2)}\left[\frac{\alpha_m^{(2,1)}(3\cos^2\psi - 1) + \alpha_m^{(2)}3\sin\psi\cos\psi}{4\pi d^3}\right] \tag{75}$$

$$\tilde{\alpha}_m^{(1,2)} \simeq \alpha_m^{(1,2)}\left[1 - \frac{\alpha_m^{(1,2)}3\sin\psi\cos\psi + \alpha_m^{(1)}(3\cos^2\psi - 1)}{4\pi d^3}\right]^{-1}$$

$$+ \frac{\alpha_m^{(1,2)}\alpha_m^{(2)}(3\sin^2\psi - 1) + \alpha_m^{(1)}\alpha_m^{(2)}3\sin\psi\cos\psi}{4\pi d^3} \tag{76}$$

$$\tilde{\alpha}_m^{(2,1)} \simeq \alpha_m^{(2,1)}\left[1 - \frac{\alpha_m^{(2,1)}3\sin\psi\cos\psi + \alpha_m^{(2)}(3\sin^2\psi - 1)}{4\pi d^3}\right]^{-1}$$

$$+ \frac{\alpha_m^{(2,1)}\alpha_m^{(1)}(3\cos^2\psi - 1) + \alpha_m^{(2)}\alpha_m^{(1)}3\sin\psi\cos\psi}{4\pi d^3}\,. \tag{77}$$

The values for symmetric apertures take on a particularly simple form,

$$\tilde{\alpha}_e = \alpha_e\left[1 - \frac{\alpha_e}{4\pi d^3}\right]^{-1} \tag{78}$$

$$\tilde{\alpha}_m^{(1)} = \alpha_m^{(1)}\left[1 - \frac{\alpha_m^{(1)}(3\cos^2\psi - 1)}{4\pi d^3}\right]^{-1} \tag{79}$$

$$\tilde{\alpha}_m^{(2)} = \alpha_m^{(2)}\left[1 - \frac{\alpha_m^{(2)}(3\sin^2\psi - 1)}{4\pi d^3}\right]^{-1} \tag{80}$$

$$\tilde{\alpha}_m^{(1,2)} = \frac{\alpha_m^{(1)}\,\alpha_m^{(2)}\,3\sin\psi\cos\psi}{4\pi d^3} \tag{81}$$

$$\tilde{\alpha}_m^{(2,1)} = \tilde{\alpha}_m^{(1,2)} \tag{82}$$

for $\alpha_m^{(1,2)} = \alpha_m^{(2,1)} = 0$. We note that for symmetric apertures the electric dipole moment is always increased by the presence of a second aperture. However, the magnetic dipole moments may be either increased or decreased depending upon the relative orientation of the two apertures. Therefore, the total dipole moments or the energy transmission per aperture can be either increased or decreased due to the coupling or interaction of a second aperture. The dominant polarizability $\tilde{\alpha}_m^{(1)}$ $\left(\tilde{\alpha}_m^{(2)}\right)$ takes on a maximum (minimum) value at $\psi = 0,\pi$ and a minimum (maximum) value at $\psi = \pm\pi/2$. At $\psi = \pm 54.7°$ and $180° \pm 54.7°$, $\tilde{\alpha}_m^{(1)} = \alpha_m^{(1)}$. At $\psi = \pm 90° \pm 54.7°$, $\tilde{\alpha}_m^{(2)} = \alpha_m^{(2)}$. The cross polarizabilities $\tilde{\alpha}_m^{(1,2)}$ and $\tilde{\alpha}_m^{(2,1)}$ take on positive values for ψ in the first and third quadrants and negative values for ψ in the second and fourth quadrants. The change in polarizability due to coupling is small for circular apertures. For example, in the case $d/a = 3$, find $\tilde{\alpha}_e \simeq 1.008\ \alpha_e$, $\tilde{\alpha}_m^{(1)} = 1.032\ \alpha_m^{(1)}$ and $\tilde{\alpha}_m^{(2)} = .984\ \alpha_m^{(2)}$ when $\psi = 0$. Thus, the correction due to interaction of the circular apertures is, at most, on the order of a few percent unless $d/a \to 2$. This supports our initial assumption that only the near-field terms are needed in the coupling calculation. We note that the coupling may become considerably larger than this for particular orientations of two noncircular apertures.

An alternative way to think about the coupling is to consider the induced dipole moments. We can write the total dipole moment $\underline{p}$ for the shadow side of the screen as

$$\underline{p} = -\underline{p}^{o} + \underline{p}^{ind} \tag{83}$$

where $\underline{p}^{o}$ is the original dipole moment for the illuminated side of the screen and $\underline{p}^{ind}$ is the induced dipole moment for the shadow side of the screen (See figure 1). Note that $\underline{p}^{ind}$ is caused by $\underline{p}^{o}$. The symbol $\underline{p}$ refers to $\underline{p}_e$, $\underline{p}_m^{(1)}$ or $\underline{p}_m^{(2)}$. Figure 17 shows the various dipole moments that can be induced in the aperture plane. It is apparent that the largest induced magnetic dipole moment, and hence the largest interaction, occurs when the line connecting the two apertures is along the incident magnetic field. In this case the induced magnetic dipole moment is parallel to the original magnetic dipole moment $-\underline{p}_o$. The induced and original magnetic moments are antiparallel when the incident magnetic field is perpendicular to the line connecting the two apertures, but the interaction is smaller than in the previous case. We have again ignored the unimportant magnetic (electric) dipole moments which are due to the electric (magnetic)interaction field.

No fundamentally new phenomena are introduced with regard to energy distribution or transmission coefficient over that found for noncircular apertures. That is, the results of the previous section can be used directly (for each aperture) by the following formal substitution

$$\begin{aligned} \alpha_m^{(1)} \sin\chi &\to \tilde{\alpha}_m^{(1)} \sin\chi - \tilde{\alpha}_m^{(1,2)} \cos\chi \\ \alpha_m^{(2)} \cos\chi &\to \tilde{\alpha}_m^{(2)} \cos\chi - \tilde{\alpha}_m^{(2,1)} \sin\chi \end{aligned} \tag{84}$$

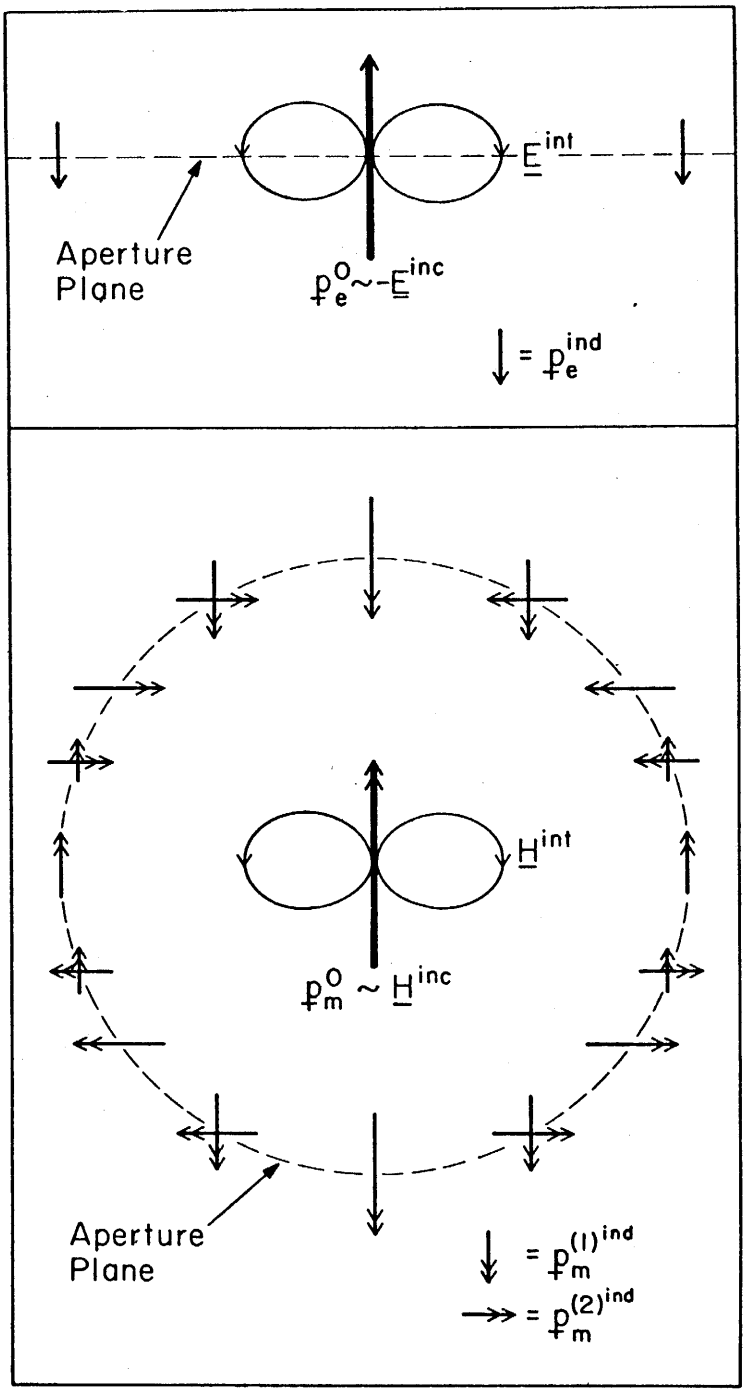

Figure 17. Electric Dipole Moments $\underline{p}_e^{ind}$ Induced by the Interaction Electric Field $\underline{E}^{int}$ and the Magnetic Dipole Moments $\underline{p}_m^{ind}$ Induced by the Interaction Magnetic Field $\underline{H}^{int}$.

This brings about still another equivalent method of viewing aperture coupling. For circular apertures and $\psi = 0$ or $\pi/2$, it is known that $\tilde{\alpha}_m^{(1,2)} = \tilde{\alpha}_m^{(2,1)} = 0$. Thus, for this case the coupling only changes the values of $\tilde{\alpha}_m^{(1)}$, $\tilde{\alpha}_m^{(2)}$ and $\tilde{\alpha}_e$ away from the uncoupled values $\alpha_m^{(1)}$, $\alpha_m^{(2)}$ and α_e. This is identical to changing the eccentricity away from zero. Interestingly, for $\psi = 0$ (i.e., apertures along $\hat{e}_{||}$), the coupled circular apertures are equivalent to uncoupled elliptical apertures with their major axis along $\hat{e}_{||}$. For $\psi = \pi/2$ (i.e., apertures along $\hat{e}_{\perp}$) the coupled circular apertures are equivalent to uncoupled elliptical apertures with their major axis along $\hat{e}_{\perp}$. A sketch is shown in figure 18. The equivalent eccentricity depends upon the orientation of the incident field and further calculations will not be given here. However, we note that in general we can think of coupling as increasing the eccentricity and/or asymmetry of the aperture in such a way that relative elongation appears along a line parallel to that joining the apertures.

Before considering the case of more than two apertures, we should state explicitly the approximations that were used to derive the coupling formulas. First, we assumed that the near fields of the aperture were just the near fields of the dipole. This point was taken up earlier in the second section where it was shown that for the circular aperture the dipole fields closely approximated the exact field for $r = d \gtrsim 2a$ (see figure 4). However, the average field over the aperture is considerably larger than the dipole field as $d \to 2a$. Thus the coupling is somewhat underestimated for $2a < d < 3a$. However, for $d \gtrsim 3a$ the dipole field is adequate. We assume that for noncircular apertures the dipole approximation holds for $d \gtrsim 1.5L$, where L is a typical aperture dimension. To get more exact values for small d, one could use a local radius of curvature

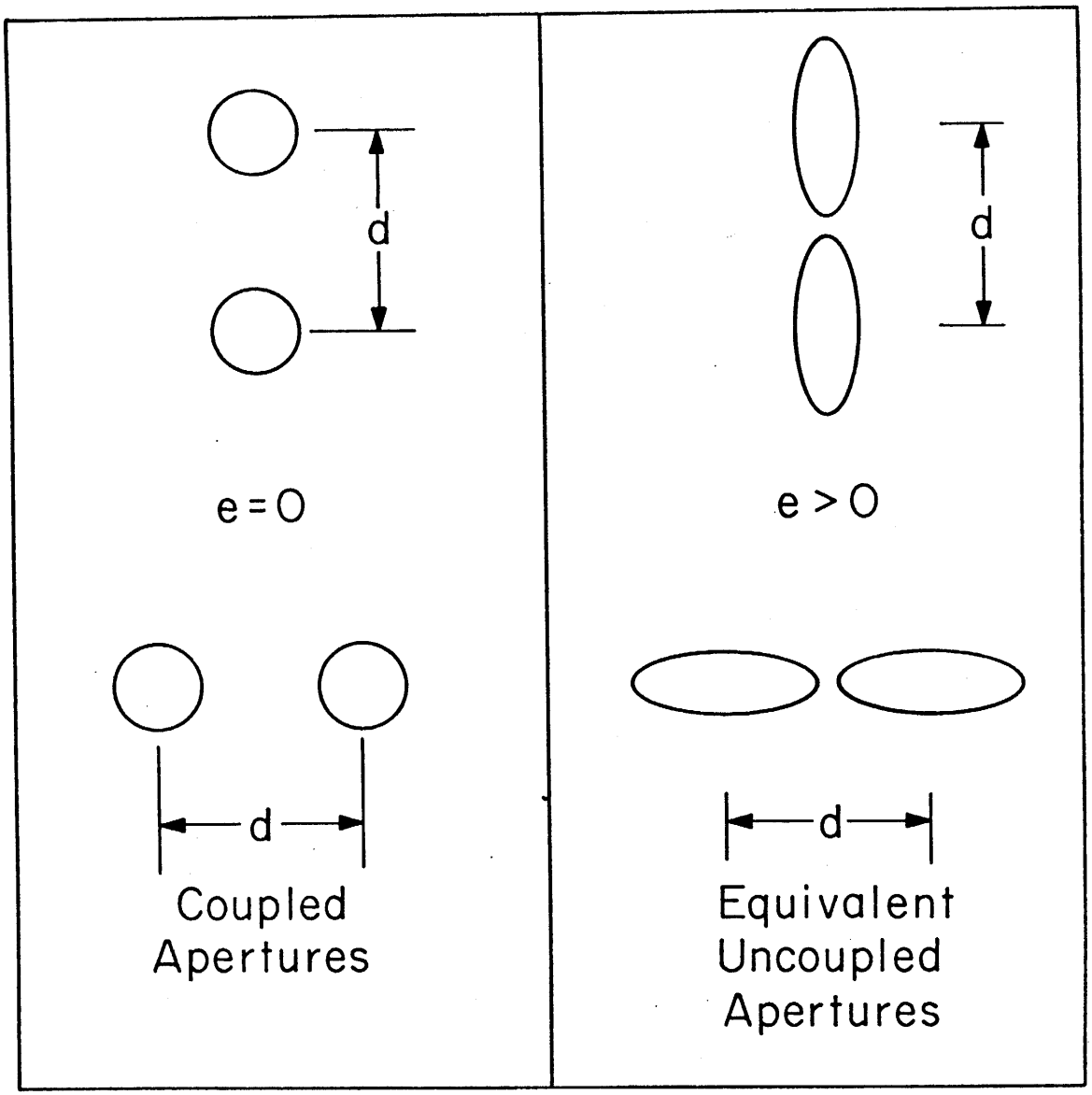

Figure 18. Sketch which Demonstrates the Equivalence of Aperture Coupling and Increased Eccentricity.

of the aperture edge as a value for the radius a, and use that result in the exact expression for the fields of a circular aperture (see refs. [2,3] or equation (16) or figure 4).

In the second approximation we neglected the intermediate and far fields in calculating the interaction fields. This is almost always justified because the coupling is usually small even for closely spaced apertures. If phase effects are important, however, the static approximation given in (67-69) can be replaced by the exact expressions given by (50-55). In this case the polarizabilities would become complex.

The third approximation involved elimination of higher order terms in polarizability/(distance)^3. This assumes that the interaction is small. Since this is almost always true, it is not necessary to give the exact expressions for the polarizabilities. However, the calculation is straightforward and can be found directly from equations (64-72).

In the fourth approximation we assumed that the interaction field was constant over the aperture. As is true for most of the other approximations, this approximation only breaks down for $d \lesssim 1.5L$. The correction for nonuniform fields has been given by Eggimann for the special case of circular apertures [17].

In this section we have given simple expressions for the coupling between two apertures of arbitrary shape. This coupling can be thought of as due to equivalent polarizabilities, induced dipoles, or changes in symmetry and eccentricity. In general the coupling produces crossed magnetic polarizabilities and either increases or decreases the dominant magnetic polarizabilities and increases the electric polarizabilities.

Thus the transmission coefficient for each aperture may be either increased or decreased. This change is typically 10% for circular apertures spaced approximately 3 radii apart. When the incident magnetic field is parallel to the line connecting the apertures, the transmission per aperture is increased. When the incident magnetic field is perpendicular to the line connecting the apertures the transmission is decreased. The simple results given in this section are valid for $1.5L \lesssim d \lesssim 0.5\lambda$ but may be fixed up to account for other separation distances. Further work needs to be done to find exact solutions for coupling between closely spaced elongated apertures.

SECTION V
TRANSMISSION THROUGH MANY SMALL APERTURES

The results of the previous section can be generalized to include the case of transmission through and coupling among many small apertures. The configuration that we will consider is shown in figure 19. A row of N apertures of arbitrary shape are spaced a distance d apart and are oriented along the array line which makes an angle ψ with respect to the $\hat{e}_{||}$ axis. In this section, two effects need to be calculated. First, there are interactions or coupling among all the apertures. The expressions found previously for the polarizabilities and induced dipole moments will be slightly modified. Second, the radiation pattern of the array of apertures will have to be found. In the previous section, with only two apertures and $kd \ll 1$, the far-field energy distribution was similar to that of a single aperture. However, if $Nkd \gtrsim 1$, then phase effects along the array will become important and the distribution pattern of one aperture needs to be multiplied by an appropriate array factor AF which accounts for the N apertures. We now consider each of these problems in detail.

The most significant coupling effect upon any given aperture is due to the adjacent apertures. Since the interaction fields (67-69) are the same for $\psi = \psi'$ and $\psi = \psi' + \pi$, the effect of adjacent apertures is to double the coupling or the induced dipole moments. Other non-adjacent apertures will have less effect. To include all of these additional couplings we can make the substitution for the q^{th} aperture

$$1/d^3 \rightarrow C_q/d^3$$

in the formulas for the polarizabilities (73-81). C_q is now the effective

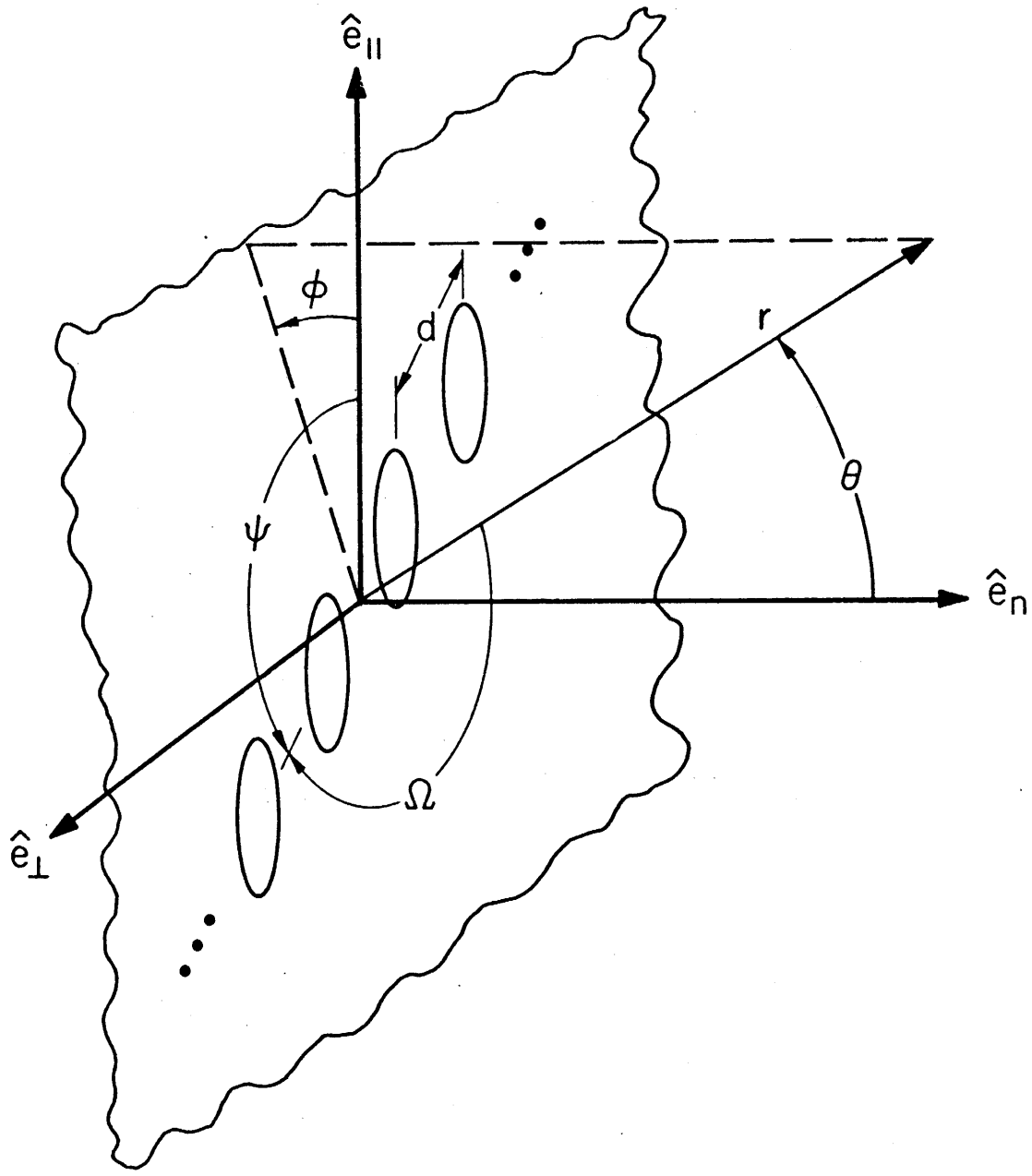

Figure 19. Geometry of a Row of N Apertures Spaced a Distance d Apart. The aperture array line makes an angle ψ with $\hat{e}_{\parallel}$ and an angle Ω with r .

coupling coefficient of the q^{th} aperture which accounts for the couplings due to all other apertures. Thus, find

$$\underline{p}_{e_q} = \underline{p}_e(\tilde{\alpha}_{e_q})$$

$$\underline{p}_{m_q}^{(1)} = \underline{p}_m^{(1)}(\tilde{\alpha}_{m_q}^{(1)}\tilde{\alpha}_{m_q}^{(1,2)}) \tag{85}$$

$$\underline{p}_{m_q}^{(2)} = \underline{p}_m^{(1)}(\tilde{\alpha}_{m_q}^{(2)}, \alpha_{m_q}^{(2,1)})$$

where

$$\tilde{\alpha}_{e_q} \simeq \alpha_e\left[1 - \frac{C_q\alpha_e}{4\pi d^3}\right]^{-1} \tag{86}$$

$$\tilde{\alpha}_{m_q}^{(1)}_{2} \simeq \alpha_m^{(1)}_{2}\left\{1 - C_q\left[\frac{\alpha_m^{(1)}_{2}\left[3\begin{pmatrix}\cos^2\psi\\ \sin^2\psi\end{pmatrix} - 1\right] + \alpha_m^{(1,2)}_{(2,1)}\ 3\sin\psi\cos\psi}{4\pi d^3}\right]\right\}^{-1}$$

$$+ C_q\alpha_m^{(2,1)}_{(1,2)}\left[\frac{\alpha_m^{(1,2)}_{(2,1)}\left[3\begin{pmatrix}\sin^2\psi\\ \cos^2\psi\end{pmatrix} - 1\right] + \alpha_m^{(1)}_{2}\ 3\sin\psi\cos\psi}{4\pi d^3}\right] \tag{87}$$

$$\tilde{\alpha}_{m_q}^{(1,2)}_{(2,1)} \simeq \alpha_m^{(1,2)}_{(2,1)}\left\{1 - C_q\left[\frac{\alpha_m^{(1,2)}_{(2,1)}\ 3\sin\psi\cos\psi + \alpha_m^{(1)}_{2}\left(3\begin{pmatrix}\cos^2\psi\\ \sin^2\psi\end{pmatrix} - 1\right)}{4\pi d^3}\right]\right\}^{-1}$$

$$+ C_q\left[\frac{\alpha_m^{(1,2)}_{(2,1)}\alpha_m^{(2)}_{1}\left[3\begin{pmatrix}\sin^2\psi\\ \cos^2\psi\end{pmatrix} - 1\right] + \alpha_m^{(1)}\alpha_m^{(2)}\ 3\sin\psi\cos\psi}{4\pi d^3}\right]. \tag{88}$$

Using the methods and approximations of the previous section we can evaluate the effective coupling coefficient,

$$C_q = \sum_{n=1}^{q-1}\frac{1}{n^3} + \sum_{n=1}^{N-q}\frac{1}{n^3} \tag{89}$$

The upper bound for C_q $(q \neq 1,N)$ is

$$C_{q_{max}} \xrightarrow{N\to\infty} 2\zeta(3) = 2.4041 \ldots \tag{90}$$

where $\zeta(n)$ is the Riemann zeta function. The lower bound for C_q $(q \neq 1,N)$ is

$$C_{q_{min}} \xrightarrow{N\to 2} 2 \tag{91}$$

The bounds for $C_1 = C_N$ are one-half the values given by (90-91). Thus we can write

$$2 \leq C_q \leq 2.4041 \ldots \qquad (q \neq 1,N) \tag{92}$$

$$1 \leq C_q \leq 1.2021 \cdots \qquad (q = 1,N) \tag{93}$$

For N = 5, the upper bounds of (92-93) produce values that are approximately 6% too large. The upper bound becomes more accurate for N > 5. Thus, for a large number of apertures, we can use the approximation

$$C_q \simeq C = 2.4 \qquad (q = 1,2,\cdots N) \tag{94}$$

with little error. For circular apertures spaced a distance d = 3a apart we find $\tilde{\alpha}_e \simeq 1.020\ \alpha_e$, $\tilde{\alpha}_m^{(1)} \simeq 1.078\ \alpha_m^{(1)}$ and $\tilde{\alpha}_m^{(2)} \simeq .961\ \alpha_m^{(2)}$ when $\psi = 0$. For $\psi = \pi/2$ we find $\tilde{\alpha}_e \simeq 1.020\ \alpha_e$, $\tilde{\alpha}_m^{(1)} \simeq .961\ \alpha_m^{(1)}$ and $\tilde{\alpha}_m^{(2)} = 1.078\ \alpha_m^{(2)}$. This implies that the change in transmitted energy due to the coupling will be~10% for apertures with zero eccentricity which are spaced $d \gtrsim 1.5L$ apart. As before, we note that for very closely spaced apertures or apertures of large eccentricity, the change in transmitted energy could be considerably larger than 10%.

The problem of radiation from many apertures is now reduced to the well-known problem of radiation from many dipole moments. The dipole moments in the field expressions (50-55) should be replaced by the following expression for N even:

$$\underline{p} \rightarrow \sum_{q=1}^{N/2} \underline{p}_q \, e^{i[k(2q-1)d \cos \Omega]/2} + \underline{p}_q \, e^{-i[k(2q-1)d \cos \Omega]/2} \tag{95}$$

where $\cos \Omega = \sin \theta \cos \psi$ (see figure 19) and where $\underline{p}_q$ may be either $\underline{p}_{e_q}$, $\underline{p}_{m_q}^{(1)}$ or $\underline{p}_{m_q}^{(2)}$. A similar expression can be written for N odd. The problem is now solved. However, a useful approximation occurs for the case of large N. For the case of many apertures, we can replace C_q by $C \simeq 2.4$ and sum the series given in (95). Thus we have

$$\underline{p} \xrightarrow[N \text{ large}]{} \underline{p} \, AF \tag{96}$$

where

$$AF \simeq \frac{\sin(N\Omega/2)}{\sin \Omega/2} \tag{97}$$

and again $\underline{p}$ may be $\underline{p}_e$, $\underline{p}_m^{(1)}$ or $\underline{p}_m^{(2)}$. AF is the array factor which adapts the results of radiation from a single aperture to the case of radiation from many apertures. Many examples of the use of the array factor are given in the references [8,9,11,14]. We note here that the fields given previously (50-55) should be multiplied by AF to go from the result N = 1 to N large. Similarly the far-field energy distribution given in (56) and shown in figures 10-11 should be multiplied by $|AF|^2$ for N large.

In this section we show the changes that are needed to convert the single-aperture expressions into the expressions for many coupled apertures. The coupling is calculated in the static approximation as before. The phase effects along the aperture array are taken into account in an exact manner. A simple result for the fields and energy distribution is found under the approximation that the coupling between each aperture is identical. The total change in transmitted energy due to coupling among apertures is on the order of 10% or less if the apertures are spaced at least three radii apart. When the magnetic field is parallel to the line of the array the transmitted energy is decreased. The transmitted energy is increased when the magnetic field is perpendicular to the line of the array.

SECTION VI

AN APPLICATION

The previous sections contain calculations and expressions for the general case of arbitrary incidence. In shielding problems it is often of interest to have simple expressions which describe the aperture under the conditions of maximum transmission. For the case of polarized waves maximum transmission occurs for grazing incidence when the magnetic field is aligned with the major axis of the aperture. For aperture arrays, maximum transmission occurs for grazing incidence with the magnetic field aligned with the array axis (for apertures with small eccentricity) or with the magnetic field along the major axis of the aperture (for apertures with large eccentricity). For unpolarized waves, maximum transmission occurs for normal incidence. The simplified formulas for maximum transmission will be denoted by the subscript "max" and will be given in the first portion of this section. The second part will contain a numerical example.

For grazing incidence with the magnetic field along the maor axis of the aperture (i.e., $\alpha_m^{(1)} \geq \alpha_m^{(2)}$, $\chi = \pi/2$, $\alpha = \pi/2$, $\beta = 0$) we find the far-field energy distribution from equation (56) as

$$\left(\frac{w^{tr}}{w^{inc}}\right)_{max} = \frac{k^4}{16\pi r^2}\left[\alpha_e^2 \sin^2\theta + 2\alpha_e\alpha_m^{(1)}\sin\phi\sin\theta + \alpha_m^{(1)2}(1 - \cos^2\phi\sin^2\theta)\right] \qquad (98)$$

The transmission coefficient becomes

$$\tau_{max} = \frac{k^4}{12\pi A}\left[\frac{\alpha_e^2 + \alpha_m(1)^2}{\cos\gamma}\right] \tag{99}$$

from (59). The maximum transmission coefficient for unpolarized waves occurs for normal incidence (i.e., $\alpha = \beta = \gamma = 0$) and is given by (62)

$$\langle\tau\rangle_{max} = \frac{k^4}{24\pi A}\left[\alpha_m(1)^2 + \alpha_m(2)^2\right] \tag{100}$$

Upper bounds for the transmission coefficients can be given explicitly by combining (60) with (99) and (100). We find

$$\tau_{max} \leq \frac{68(P/\lambda)^6}{27\pi^3\cos\gamma(A/\lambda^2)} \tag{101}$$

$$\langle\tau\rangle_{max} \leq \frac{64(P/\lambda)^6}{27\pi^3(A/\lambda^2)} \tag{102}$$

for the cases of polarized and unpolarized waves, respectively. For completeness, we repeat the coupling formulas for apertures with lines of symmetry as given in (86)-(88).

$$\tilde{\alpha}_e = \alpha_e\left[1 - C_q\frac{\alpha_e}{8\pi d^3}\right]^{-1} \tag{103}$$

$$\tilde{\alpha}_m(1) = \alpha_m(1)\left[1 - C_q\frac{\alpha_m(1)(3\cos^2\psi - 1)}{8\pi d^3}\right]^{-1} \tag{104}$$

$$\tilde{\alpha}_m(2) = \alpha_m(2)\left[1 - C_q\frac{\alpha_m(2)(3\sin^2\psi - 1)}{8\pi d^3}\right]^{-1} \tag{105}$$

$$\tilde{\alpha}_m(1,2) = C_q\frac{\alpha_m(1)\alpha_m(2)3\sin\psi\cos\psi}{8\pi d^3} = \tilde{\alpha}_m(2,1) \tag{106}$$

Consider now the following numerical example. We want to calculate the equivalent polarizabilities and maximum transmission coefficient for a polarized wave which is incident upon an infinite array of rectangular apertures spaced 50.8 cm apart and of size 25.4 cm by 35.6 cm. The array line is parallel to the smaller side of the aperture. This means that the eccentricity, spacing, area, perimeter and array angle are given by

$$e = .701 \tag{107}$$

$$d = 0.508 \text{ m} \tag{108}$$

$$A = .0904 \text{ m}^2 \tag{109}$$

$$P = 1.22 \text{ m} \tag{110}$$

$$\chi = \pi/2 \tag{111}$$

From figures 8 and 9 or from Latham [12] we find

$$\alpha_e = 1.808A^2/P = 1.21 \times 10^{-2} \text{ m}^3 \tag{112}$$

$$\alpha_m^{(1)} = 5.503A^2/P = 3.69 \times 10^{-2} \text{ m}^3 \tag{113}$$

$$\alpha_m^{(2)} = 3.335A^2/P = 2.23 \times 10^{-2} \text{ m}^3 \tag{114}$$

Upon substitution of (108), (111) and (112)-(114) into (103)-(106) we calculate

$$\tilde{\alpha}_e = 1.22 \times 10^{-2} \text{ m}^3 \tag{115}$$

$$\tilde{\alpha}_m^{(1)} = 3.59 \times 10^{-2} \text{ m}^3 \tag{116}$$

$$\tilde{\alpha}_m^{(2)} = 2.27 \times 10^{-2} \text{ m}^3 \tag{117}$$

$$\tilde{\alpha}_m^{(1,2)} = \tilde{\alpha}_m^{(2,1)} = 0 \tag{118}$$

where we have used the fact $C_q = 2.404$. Note that the polarizabilities change at the most by less than 3% due to coupling. The maximum transmission coefficient per aperture is given by a generalization of (99) with the result

$$\tau_{max} = \frac{k^4}{12\pi A}\left[\frac{\tilde{\alpha}_e^2 + \tilde{\alpha}_m(1)^2}{\cos\gamma}\right] = \frac{0.657}{\lambda^4\cos\gamma} \qquad (119)$$

under the assumption $\lambda >> 0.3$ m. The value for τ_{max} without the coupling taken into consideration is approximately 5% larger than the value shown in (19). The upper bound given by (101) is easily satisfied by (119). A straightforward calculation indicates that the above value for maximum transmission can be reduced by $\sim$40% if circular apertures (of the same area) were to replace the reactangular apertures.

In this section the formulas for worst-case shielding calculations are gathered together. These results are then applied to a simple numerical calculation. The calculation parameters used here model the windows along the fuselage of the E-4 aircraft.

SECTION VII
CONCLUSIONS

In this report we have examined energy transmission through one or more small apertures of arbitrary shape. We list several major conclusions:

1. Electric and magnetic dipole moments will be induced in apertures by normal electric and tangential magnetic incident fields.
2. For circular holes, maximum energy transmission occurs for parallel polarization and grazing incidence.
3. The maximum near-field energy distribution occurred at the aperture plane for all polarizations and angles of incidence.
4. For noncircular apertures, maximum energy transmission occurs for grazing incidence when the magnetic field is aligned with the major axis of the aperture.
5. The largest amount of far-field energy occurred in a direction opposite to that of the incident wave vector for grazing incidence.
6. Inner and outer radii can be defined and used to give lower and upper bounds for the electric and mean magnetic polarizabilities; from these polarizabilities, bounds can be placed on the transmission coefficient.
7. Accurate approximations can be given for the transmission of unpolarized waves through apertures of arbitrary shape; the ordering of aperture transmission according to shape is identical to the ordering of the perimeters for a given area.
8. Simple expressions are found for the coupling between two or more apertures; the coupling increases the energy transmission

when the line of apertures is parallel to the incident magnetic field and decreases the energy transmission when the line of apertures is perpendicular to the incident magnetic field.

9. For apertures spaced at distances larger than five times a typical dimension, the coupling is negligible ($\lesssim$ 1%).
10. For a large number of equally spaced circular apertures, the coupling changes the total transmitted energy by less than 10% for aperture spacings equal to or greater than three aperture radii; larger changes may be possible for apertures of large eccentricity and/or for apertures of very close spacing.

Through the first part of this report we have seen that simple geometric considerations can extend the results for the transmitted fields of circular apertures to the case of transmission through convex apertures of arbitrary shape. The second part of this report extended the results of single apertures to many apertures through the use of static coupling techniques and array theory. Further work needs to be done on the problem of very closely spaced apertures and on finding more accurate approximations for the transmission of polarized waves through noncircular apertures. The problem of apertures in nonplanar electrical walls is also open to investigation.

APPENDIX

This appendix contains several tables of parameter values which were used in the main body of this report. Some of the tables correspond directly to parameters plotted in the figures.

Table 1.

GEOMETRIC RELATIONS FOR ELLIPSE, RECTANGLE, TRIANGLE AND RHOMBUS (FIGURES 7 AND 14). THE SYMBOLS e , A AND P REPRESENT THE ECCENTRICITY, AREA AND PERIMETER, RESPECTIVELY.

Shape	e	A	P
ELLIPSE a = semimajor axis b = semiminor axis	$\sqrt{1 - b^2/a^2}$	πab	$4aE(e^2) = 4\sqrt{A/\pi}\, E(e^2)(1-e^2)^{-1/4}$
RECTANGLE d = width ℓ = length	$\sqrt{1 - d^2/\ell^2}$	ℓd	$2(\ell+d) = 2\sqrt{A}\,[(1-e^2)^{1/4} + (1-e^2)^{-1/4}]$
RHOMBUS h = height b = base a = length of side	$\sqrt{1 - h^2/b^2}$	$bh/2$	$4a = 2\sqrt{2A}\sqrt{2-e^2}\,(1-e^2)^{-1/4}$
TRIANGLE h = height b = base a = length of side	$\sqrt{1 - 3/4h^2/b^2}$	$bh/2$	$2a+b = 2\sqrt{A}\,[\sqrt{1 + 3(1-e^2)} + 1][3(1-e^2)]^{-1/4}$

Table 2.

VALUE OF PERIMETER/AREA$^{1/2}$ FOR VARIOUS ECCENTRICITIES AND SHAPES.

$P/A^{1/2}$

e	ELLIPSE	RECTANGLE	RHOMBUS	TRIANGLE
0	3.544	4.000	4.000	4.559
.2	3.545	4.000	4.000	4.559
.4	3.550	4.004	4.008	4.566
.6	3.578	4.025	4.050	4.602
.7	3.620	4.057	4.113	4.659
.8	3.718	4.131	4.258	4.791
.85	3.818	4.207	4.405	4.928
.9	4.006	4.350	4.673	5.186
.95	4.453	4.697	5.303	5.811
.99	6.015	6.076	7.605	8.211

Table 3.

VALUES FOR NORMALIZED $(\alpha/A^{3/2})$ POLARIZABILITIES AND INTERMEDIATE QUANTITIES USED IN CALCULATIONS INVOLVING ELLIPTICAL APERTURES.

e	$(1-e^2)$	$E(e^2)$	$K(e^2)$	$\alpha/A^{3/2}$		
				$\alpha_e/A^{3/2}$	$\alpha_m^{(1)}/A^{3/2}$	$\alpha_m^{(2)}/A^{3/2}$
0	1.0000	1.567	1.571	.4789	.9578	.9578
.2	.9600	1.555	1.587	.4789	.9726	.9433
.4	.8400	1.506	1.640	.4782	1.023	.8978
.6	.6400	1.418	1.751	.4745	1.138	.8139
.7	.5100	1.356	1.846	.4689	1.246	.7517
.8	.3600	1.276	1.995	.4565	1.443	.6694
.85	.2775	1.228	2.110	.4446	1.612	.6139
.9	.1900	1.172	2.281	.4239	1.909	.5448
.95	.0975	1.103	2.591	.3812	2.615	.4462
.99	.0199	1.029	3.156	.2747	6.540	.2867

Table 4.

VALUES FOR NORMALIZED ($\alpha\ P/A^2$) POLARIZABILITIES OF ELLIPTICAL AND RECTANGULAR APERTURES. VALUES FOR RECTANGULAR APERTURES ARE TAKEN FROM THE NUMERICAL WORK OF LATHAM [12] (FIGURES 8 - 9).

$\alpha P/A^2$

	ELLIPSE			RECTANGLE		
e	$\alpha_e P/A^2$	$\alpha_m^{(1)} P/A^2$	$\alpha_m^{(2)} P/A^2$	$\alpha_e P/A^2$	$\alpha_m^{(1)} P/A^2$	$\alpha_m^{(2)} P/A^2$
0	1.698	3.395	3.395	1.82	4.2	4.2
.2	1.698	3.448	3.344	1.82	4.2	4.2
.4	1.698	3.632	3.187	1.81	4.4	3.8
.6	1.698	4.071	2.912	1.81	4.9	3.6
.7	1.698	4.512	2.722	1.80	5.5	3.3
.8	1.698	5.363	2.489	1.80	6.4	3.0
.85	1.698	6.155	2.344	1.78	7.6	2.8
.9	1.698	7.647	2.182	1.76	8.8	2.5
.95	1.698	11.65	1.987	1.74	13.	2.2
.99	1.698	40.42	1.772	1.58	32.	1.9

Table 5.

VALUES OF NORMALIZED TRANSMISSION COEFFICIENT ($\tau \cos \gamma / k^4 A^2$) FOR POLARIZED WAVE INCIDENT UPON AN ELLIPTIC APERTURE OF VARYING ECCENTRICITY (FIGURE 12 AND (62)).

$$\frac{\tau \cos \gamma}{k^4 A^2}$$

	Normal Incidence			Grazing Incidence		
e	$\chi = 0$	$\chi = \pi/4$	$\chi = \pi/2$	$\chi = 0$	$\chi = \pi/4$	$\chi = \pi/2$
0	2.432×10^{-2}	2.432×10^{-2}	2.432×10^{-2}	3.040×10^{-2}	3.040×10^{-2}	3.040×10^{-2}
.2	2.360	2.435	2.504	2.968	3.043	3.117
.4	2.138	2.458	2.777	2.745	3.065	3.384
.6	1.757	2.595	3.433	2.354	3.192	4.030
.7	1.499	2.810	4.121	2.082	3.393	4.704
.8	1.188	3.357	5.525	1.741	3.910	6.078
.85	.9996	3.946	6.892	1.524	4.420	7.416
.9	.7873	5.229	9.671	1.264	5.706	10.15
.95	.5282	9.334	18.14	.9137	9.719	18.53
.99	.2181	56.86	113.5	.4182	57.06	113.7

Table 6.

APPROXIMATE VALUES OF NORMALIZED TRANSMISSION COEFFICIENT ($\langle\tau\rangle \cos\gamma / k^4 A^2$) FOR UNPOLARIZED WAVES AND SEVERAL APERTURES OF DIFFERENT SHAPE AND ECCENTRICITY (FIGURE 15 AND (63)). THE FIELDS ARE NORMALLY INCIDENT UPON THE APERTURE.

$$\frac{\langle\tau\rangle \cos\gamma}{k^4 A^2}$$

e	ELLIPSE	RECTANGLE	RHOMBUS	TRIANGLE
0	2.432×10^{-2}	5.023×10^{-2}	5.023×10^{-2}	11.01×10^{-2}
.2	2.435	5.024	5.026	11.01
.4	2.454	5.052	5.084	11.11
.6	2.573	5.213	5.409	11.65
.7	2.761	5.466	5.935	12.53
.8	3.242	6.096	7.311	14.84
.85	3.802	6.811	8.954	17.57
.9	5.066	8.305	9.826	23.85
.95	9.566	13.16	27.26	47.23
.99	58.05	61.71	237.3	375.9

REFERENCES

[1] H. A. Bethe, "Theory of Diffraction by Small Holes", Phys. Rev. 66, 163-182 (1942).

[2] C. J. Bouwkamp, "On Bethe's Theory of Diffraction by Small Holes", Philips Res. Rep. 5, 321-332 (1950).

[3] C. J. Bouwkamp, "On the Diffraction of Electromagnetic Waves by Small Circular Disks and Holes", Philips Res. Rep. 5, 401-422 (1950).

[4] J. Meixner and W. Audrejewski, "Strenge Theorie der Beugung ebener Elektromagnetischer Wellen an der Vollkommen Leitenden Kreisscheibe und an den Kreisförmigen Öffnung im Vollkommen Leitenden ebenen Schirm, Ann. Physik 7, 157-168 (1950).

[5] C. J. Bouwkamp, "A Note on Singularities Occurring at Sharp Edges in Electromagnetic Diffraction Theory", Physica 12, 467-474 (1946).

[6] J. Meixner, "The Behavior of Electromagnetic Fields at Edges", Inst. Math. Sci. Res. Rept. EM-72, New York University (December 1954).

[7] C. H. Papas, "An Application of Symmetrization to EMP Penetration Through Apertures", Interaction Note 299, December 1976.

[8] S. A. Schelkunoff and H. T. Friis, Antennas Theory and Practice, John Wiley and Sons, Inc., New York, 1952.

[9] C. H. Papas, Theory of Electromagnetic Wave Propagation, McGraw Hill, New York (1965).

[10] J. D. Jackson, Classical Electrodynamics, 2nd ed., John Wiley & Sons, New York (1975).

[11] D. S. Jones, The Theory of Electromagnetism, Macmillan, New York (1964).

[12] R. Latham, "Small Holes in Cable Shields," EMP Interaction Note 118 (Sept. 1972).

[13] C. Montgomery, R. Dicke and E. Purcell, eds, Principles of Microwave Circuits, McGraw Hill, New York (1948).

[14] R. Collin, Field Theory of Guided Waves, McGraw Hill, New York (1960).

[15] S. Cohn, "Determination of Aperture Parameters by Electrolytic-Tank Measurements," Prov. IRE 39, 1416-1421 (1951).

[16] S. Cohn, "The Electric Polarizability of Apertures of Arbitrary Shape," Proc. IRE 40, 1069-1071 (1952).

[17] W. Eggimann, "Higher-Order Evaluation of Electromagnetic Diffraction by Circular Disks," IRE Trans. Microw. Theory & Tech. MTT-9, 408-418 (1961).